Czech Technical University in Prague

Faculty of Civil Engineering

Department of Mechanics

Application of electromigration techniques in the transport of chlorides and nanoparticles in concrete

Bc. Daniel Ňachaj

Master's Thesis

Supervisor: prof. Ing. Jiří Němeček, Ph.D., DSc.

Year: Prague, 2023

ČESKÉ VYSOKÉ UČENÍ TECHNICKÉ V PRAZE
Fakulta stavební
Thákurova 7, 166 29 Praha 6

ZADÁNÍ DIPLOMOVÉ PRÁCE

I. OSOBNÍ A STUDIJNÍ ÚDAJE

Příjmení: Ňachaj Jméno: Daniel Osobní číslo: 452781

Zadávající katedra: 132 - Katedra mechaniky

Studijní program: Stavební inženýrství

Studijní obor/specializace: Konstrukce a dopravní stavby

II. ÚDAJE K DIPLOMOVÉ PRÁCI

Název diplomové práce: Uplatnění elektromigračních technik při transportu chloridů a nanočástic v betonu

Název diplomové práce anglicky: Application of electromigration techniques in the transport of chlorides and nanoparticles in concrete

Pokyny pro vypracování:
Cílem práce je prozkoumat vliv elektromigračních technik na mikrostrukturu betonu, její uplatnění pro extrakci chloridů z betonu a pro zvýšení odolnosti betonu proti pronikání chloridů pomocí injektáže nanočástic. Budou provedeny
a) akcelerované laboratorní testy,
b) testy odstraňování chloridů z betonu,
c) testy ošetřování betonu pomocí nanočástic,
d) posouzení nežádoucích účinků technik.
V práci bude provedena rešerše problematiky a série experimentů na několika typech betonů a malt. Zvláštní pozornost bude věnována porozitě betonu a vlivu elektrického proudu. Použity budou techniky MIP, SEM, XRD, TGA. Pro dané problémy bude sestaven jednoduchý analytický nebo numerický model.

Seznam doporučené literatury:
J. Němeček et al., Simulation of chloride migration in reinforced concrete, AMC 2018
J. Němeček;R. Šulc ; (...); J.Kruis, Nanoparticles in Concrete: Application in Fresh and Hardened State, Key Engineering Materials 2018
L. M. Ottosen, I. V. Christensen, I. Rörig-Dalgĺrd, et al. Utilization of electromigration in civil and environmental engineering—processes, transport rates and matrix changes. Journal of Environmental Science and Health, Part A 43(8):795–809, 2008.

Jméno vedoucího diplomové práce: prof. Ing. Jiří Němeček, Ph.D., DSc.

Datum zadání diplomové práce: 12.2.2023 Termín odevzdání DP v IS KOS: 22.5.2023
Údaj uveďte v souladu s datem v časovém plánu příslušného ak. roku

Podpis vedoucího práce Podpis vedoucího katedry

III. PŘEVZETÍ ZADÁNÍ

Beru na vědomí, že jsem povinen vypracovat diplomovou práci samostatně, bez cizí pomoci, s výjimkou poskytnutých konzultací. Seznam použité literatury, jiných pramenů a jmen konzultantů je nutné uvést v diplomové práci a při citování postupovat v souladu s metodickou příručkou ČVUT „Jak psát vysokoškolské závěrečné práce“ a metodickým pokynem ČVUT „O dodržování etických principů při přípravě vysokoškolských závěrečných prací“.

Datum převzetí zadání Podpis studenta(ky)

Declaration

I hereby declare that this master's thesis is my own work, written under supervision of prof. Ing. Jiří Němeček, Ph.D., DSc.

All sources of information that have been used in the master's thesis are acknowledged in the text and listed in the Bibliography.

In Prague, May 2023

.....
Bc. Daniel Ňachaj

Acknowledgements

Firstly, I want to express my deepest gratitude to my supervisor, prof. Jiří Němeček for his guidance, meaningful discussions and patience during the study. Also for his big help during the preparation of publications and this thesis.

My great gratitude belongs also to dr. Jiří Němeček, who always willingly helped, advised and who introduced me to all the experiments. Also for his patience during preparing articles and presentations. I would also like to thank him for his big help with this thesis.

Further, I want to thank to dr. Pavel Trávníček for his help with the python code and also his guidance during the setup of the electrical tests.

My thanks also go to doc. Martin Kepprt for his help in the preparation of thermogravimetric analysis and x-ray diffraction and for his willingness to help with interpretation of results during the study.

I would like to thank my colleagues from UCT in Prague for their help with measurements of chloride profiles. Also for their kindness, advice and help in the laboratory.

Most importantly, I would like to thank to my wife Kristiána for all her help in life and for her patience. I would also like to thank her for her great help in taking care of our daughter Emma, who never wants to sleep.

Finally, I want to thank my family for their support and for pushing me into college education, which ended up being a very interesting and educational journey.

The thesis was financially supported by the Czech Science Foundation (project No. 21-11965S) and the Grant Agency of the Czech Technical University in Prague (SGS22/001/OHK1/2T/11). Their support is gratefully acknowledged.

The work was also supported by CEMHub (Civil Engineering Materials Hub) and Scanning Electron Microscope Laboratory, CTU Prague (CE-SEM Lab) and Laboratory of Nanoindentation and Experimental Micro-Mechanics (CE-Nano Lab) at the Czech Technical University, Faculty of Civil Engineering.

Abstract

This thesis deals with the use of electromigration techniques in the study of chloride and nanoparticle transport in concrete. In particular, It focuses on the effect on porosity and chloride resistance. Various electromigration techniques, specifically direct current flow, accelerated chloride penetration, nanosilica injection and chloride extraction tests, were used. Analytical tools such as mercury intrusion porosimetry (MIP), scanning electron microscopy (SEM), image analysis, chloride profiling (grinding, leaching and potentiometric titration), thermogravimetric analysis (TGA) and X-ray diffraction (XRD) were used to determine the individual results.

Six different mixtures of concrete and mortars varying in binder type and other constituent types were studied, in order to find effects related to microstructural variations. Nanosilica injection was applied, in order to enhance concrete microstructure and to block further penetration of chlorides.

It was found that the application of electric current increases the porosity of the concrete and mortar, allowing chloride ions to penetrate more easily. These results were confirmed by the amount of total charge transferred during the electrical test, porosity measurements and chloride tests. It was also found that the process of injection of nanosilica causes higher chloride content to enter in the concrete compared to the reference sample, which is in contrast to the expected effect.

This thesis contributes to the existing knowledge on accelerated chloride and nanoparticle transport in concrete. These findings are related to topics of concrete durability, corrosion resistance and the potential consequences of different treatments used on concrete structures, such as chloride extraction or particle injection. The thesis offers practical guidelines for the experimental tests and future research directions in this area.

Keywords

concrete, mortar, cement, chlorides, electromigration, nanoparticles, nanosilica injection, transport of chlorides, accelerated tests, microstructure, C-S-H gel, scanning electron microscopy, mercury intrusion porosimetry, porosity, image analysis, chloride profile, reinforcement corrosion, thermogravimetry, x-ray diffraction, chloride penetration, chloride extraction

Abstrakt

Tato práce se zabývá využitím elektromigračních technik při studiu transportu chloridů a nanočástic v betonu. Zaměřuje se zejména na vliv na pórovitost a odolnost vůči chloridům. Byly použity různé elektromigrační techniky, konkrétně zkoušky stejnosměrným proudem, zrychlená penetrace chloridů, injektáž nanosiliky a extrakce chloridů. Pro stanovení jednotlivých výsledků byly použity analytické nástroje, jako je rtuťová intruzní porozimetrie (MIP), skenovací elektronová mikroskopie (SEM), analýza obrazu, profilování chloridů (broušení, loužení a potenciometrická titrace), termogravimetrická analýza (TGA) a rentgenová difrakce (XRD).

Bylo studováno šest různých směsí betonu a malt lišících se typem pojiva a dalšími typy složek s cílem zjistit vlivy související s mikrostrukturními změnami. Byla použita injekce nanosiliky s cílem zlepšit mikrostrukturu betonu a blokovat další pronikání chloridů.

Bylo zjištěno, že aplikace elektrického proudu zvyšuje pórovitost betonu a malty, což umožňuje snadnější pronikání chloridových iontů. Tyto výsledky byly potvrzeny množstvím celkového náboje přeneseného během zkoušky elektrickým proudem, měřením pórovitosti a zkouškami chloridů. Bylo také zjištěno, že proces injektáže nanosiliky způsobuje, že do betonu vstupuje vyšší obsah chloridů ve srovnání s referenčním vzorkem, což je v rozporu s očekávaným účinkem.

Tato práce přispívá k dosavadním poznatkům o zrychleném transportu chloridů a nanočástic v betonu. Tyto poznatky se týkají témat trvanlivosti betonu, odolnosti proti korozi a možných důsledků různých ošetření používaných na betonových konstrukcích, jako je extrakce chloridů nebo injektáž částic. Práce nabízí praktické pokyny pro experimentální zkoušky a budoucí směry výzkumu v této oblasti.

Klíčová slova

beton, malta, cement, chloridy, elektromigrace, nanočástice, vstřikování nanosiliky, transport chloridů, zrychlené zkoušky, mikrostruktura, C-S-H gel, skenovací elektronová mikroskopie, rtuťová intruzní porozimetrie, pórovitost, analýza obrazu, chloridový profil, koroze výztuže, termogravimetrie, rentgenová difrakce, penetrace chloridů, extrakce chloridů

List of Figures

List of Tables

Abbreviations

ACPT	**A**ccelerated **C**hloride **P**enetration **T**est
BSE	**B**ack-**S**cattered **E**lectrons
CET	**C**hloride **E**xtraction **T**est
CH	**C**alcium **H**ydroxide (Portladnite)
C-S-H	**C**alcium-**S**ilicate-**H**ydrate
DC	**D**irect **C**urrent
DoH	**D**egree **o**f **H**ydration
DTG	**D**erivative **T**hermo**G**ravimetry
ECE	**E**lectrochemical **C**hloride **E**xtraction
EDS	**E**nergy **D**ispersive **S**pectroscopy
HD C-S-H	**H**igh **D**ensity **C**alcium-**S**ilicate-**H**ydrate
LD C-S-H	**L**ow **D**ensity **C**alcium-**S**ilicate-**H**ydrate
MIP	**M**ercury **I**ntrusion **P**orosimetry
NS	**N**ano**S**ilica
OP	**O**pen **P**orosity
OPC	**O**rdinary **P**ortland **C**ement
PT	**P**onding **T**est
RCPT	**R**apid **C**hloride **P**ermeability **T**est
RVE	**R**epresentative **V**olume **E**lement
SE	**S**econdary **E**lectrons
SEM	**S**canning **E**lectron **M**icroscopy
TGA	**T**hermo**G**ravimetric **A**nalysis
XRD	**X**-**R**ay **D**iffraction

Contents

1 Motivation

In the construction industry, many factors are taken into consideration when assessing the condition of a structure. One of them is the corrosion of the reinforcement in concrete structures, which reduces the load bearing capacity and durability of the structure. Although the reinforcement is protected by a concrete cover layer, moisture, CO_2, harmful species like chlorides can travel through this layer. Especially in areas with increased salt concentration and on the structures where de-icing agents are used. A possible solution is to increase the chloride resistance of the concrete and mortar with the nanoparticles injection, as well as its preventive realkalisation and desalination. Both mentioned operations can be performed by accelerated electrical tests with different settings.

2 Research objectives

The aim of the thesis is to investigate the possibilities of electromigration techniques for increasing the resistance of concrete to chloride penetration and their use for:

- penetration of chlorides through concrete and mortar in a shorter time using accelerated laboratory tests with electric current,
- removal of chlorides from concretes and mortars using electric current to decrease their concentration and reduce the risk of corrosion,
- treatment of concretes and mortars with nanoparticles to increase their further resistance to chlorides and other harmful substances and thus increase their durability,
- identification of side effects of techniques affecting the microstructure that could cause undesirable effects, such as an increase of porosity.

3 Introduction

Concrete is a composite material consisting of fine and coarse aggregates bonded together with a binding component (cement paste) that hardens (cures) over time. It is the world's most common building material. It has the advantage of high compressive strength which is about ten times higher than the tensile strength. The use of concrete as the main load-bearing material in bent structures, like bridges, frames, slabs or similar structures leads to the development of tensile stresses. Reinforced concrete was invented to overcome this difficulty, where the most common and cheapest type of rebar is the steel reinforcement. The steel reinforcement performs well in tension, but on the other hand it is very prone to corrosion when exposed to corrosive environments. This undesirable property can significantly reduce the durability of concrete [1, 2].

Corrosion of reinforcement is affected by the presence of deicing salts that migrate through the microstructure and cracks from damaged concrete to the reinforcement. Corrosion of the reinforcement reduces its cross-section and reduces its load bearing capacity. Corrosion of reinforcement caused by chloride is one of the main causes of degradation of structural concrete and a factor increasing the cost to repair concrete structures. To prevent corrosion of the reinforcement and to reduce chloride/salt ingress the concrete cover is usually enlarged or the permeability of the concrete is reduced [2, 3]. In addition, a non-destructive repair methods based on electromigration are also proposed to eliminate the corrosion [4]. For example the electrochemical chloride extraction (ECE) method has been successfully used to reduce chloride attack on concrete bridges [5, 6].

The electrochemical treatment method consists in the rapid transfer of charged particles or ions into the pore structure of concrete and mortar under the influence of an electric field. Electrokinetic treatment with nanoparticles has recently been introduced to improve the microstructure of concrete and increase durability by preventing concrete porosity by filling the space with nanoparticles [7]. The treatment can also be carried out by electrochemical injection of organic corrosion inhibitors such as ethanolamine and guanidine to protect the steel reinforcement [8].

In order to improve the properties of concrete mixtures, the concrete's permeability to ions is often specified as a quality measure. Since the measurement of chloride diffusion requires a long time for their penetration or to establish steady state conditions, an electric potential is usually used to accelerate the migration of ions, greatly speeding up the process. One of the standardized electrical tests is called the Rapid Chloride Permeability Test (RCPT) according to ASTM C1202 standard [9], which is used to determine the proneness of concrete to chloride penetration [10–12].

Electrokinetic techniques are applied in several fields that allow the manipulation

of material properties. These techniques are also used for concrete, both to mitigate corrosion of reinforcement and to modify the microstructure of cement-based systems to improve their long-term properties and thus extend their overall lifetime. Electrokinetic treatment is thus used to mitigate corrosion and is proposed to refine the microstructure, increase durability, heal cracks and improve the reinforcement-concrete bond [7].

It has been found that electric current passing through the concrete can have some side effects and can increase porosity [13, 14]. Since the effect of electric current on the microstructure of the cement matrix has not been sufficiently investigated so far, it is necessary to investigate this effect further. The treatment of chloride-exposed concrete and the application of nanoparticles in general in the construction industry is a relatively unexplored and young field. Nevertheless, there are interesting and useful studies suggesting that the use of nanoparticles has a positive effect on building materials. This work therefore also focuses on the effect of electric current on the porosity and on the microstructure itself for different types of concretes and mortars treated by this method.

Some of the known nanoparticles used in construction include nano-$CaCO_3$, nano-clay, nano-TiO_2, or nano-SiO_2. The results show that nano-SiO_2, nano-$CaCO_3$ and nano-clay cause different properties such as compressive strength and acceleration of hydration or solidification time [15, 16].

Figure 3.1: A concrete bridge exposed to salt waters [17].

4 State of the art

Salt exposure is a significant problem for reinforced concrete infrastructure such as bridges, buildings and pavements. The infiltration of chloride ions resulting from the use of de-icing agents or contact with saltwater environments is harmful for these structures. The penetration of chloride ions into concrete can cause the formation of expansive corrosion products, which can lead to cracking, spalling and delamination [18–21].

Penetration of chloride into the concrete up to the reinforcing steel triggers corrosion, which disrupts the passive oxide layer that protects the steel. Oxidation of the steel creates rust that has a greater volume than the steel, leading to internal stresses that can also cause further cracking, spalling and delamination. All this contributes to the reduction of the service life of the structures and to the increase of the costs for maintenance and repair of the structures [22–25].

There are several mechanisms by which chloride ions can enter the concrete, leading to corrosion of the concrete reinforcement. These mechanisms include diffusion, absorption, conduction, or electrochemical migration. The most important mechanism of chloride ion transfer in concrete is diffusion, which is the subject of a substantial part of this paper. It occurs due to concentration gradients where ions move from areas of higher concentration to areas of lower concentration. To describe this process, Fick's laws of diffusion are commonly used. Understanding these transport mechanisms is essential to develop effective strategies to reduce salt-induced corrosion. The solution may be the use of corrosion resistant materials and active intervention methods such as extraction techniques [5, 26–30].

Electromigration techniques are methods using the application of an external electric field to induce the movement of charged particles. These techniques can be used to control the transport of chloride ions in concrete structures for a variety of purposes such as corrosion prevention, desalination and incorporation of corrosion inhibitors. Known electromigration techniques used in concrete are for example electrochemical chloride extraction, electro-osmosis, or electrokinetic nanoparticle injection [31–36].

Different methods of protection, desalination and the use of nanoparticles have been developed to deal with chloride-induced corrosion. It is possible to use corrosion-resistant reinforcement, such as stainless steel, galvanized steel or epoxy-coated steel. An example of a method of desalting a chloride-impacted structure is the above mentioned electrochemical chloride extraction method or electro-osmosis method. Incorporating nanoparticles into the concrete matrix can increase its corrosion resistance. For example, nanosilica can act as a corrosion inhibitor, blocking the transport of chloride ions and delaying the corrosion initiation [31–38].

4.1 Microstructure

The main component of concrete is cement whose microstructure is prone to electric current treatment [4]. Portland cement is composed in an approximate ratio of 5.5:2.5:1:1 mainly from C_3S (Alite), C_2S (Belite), C_3A (Aluminate), C_4AF (Ferrite). The hydration of main cement components can be described by using equations:

$$C_3S + (1.3 + x)H \longrightarrow C_{1.7}SH_x + 1.3CH, \tag{4.1}$$

$$C_2S + (0.3 + x)H \longrightarrow C_{1.7}SH_x + 0.3CH. \tag{4.2}$$

where x is an amount of water entering into the reaction, C_3S (see Eq. 4.1) primary contributes on the early stage of strength development and C_2S (see Eq. 4.2) contributes mainly on mature cement's strength development [39]. Fully hydrated portland cement contains ± 70% Calcium Silicate Hydrate (C-S-H) gels and 15 - 20% crystalline Calcium Hydroxide (CH) [40, 41].

The basic hydration chemical reactions include the formation of C-S-H gels and CH particles, also known as a Portlandite which are the main hydration products of cement paste's microstructure and also other phases of cement's microstructure such as: residual clinker, porosity, AFm, AFt and more [16].

C-S-H gels are the main bonding phases in all other Portland cement-based systems. The C-S-H gel is not a separate substance, but represents a convenient collective term for a series of quasi-amorphous particles containing CaO, SiO_2, and water that have been formed by the hydration of C_3S and C_2S in cement.

The C-S-H gel can exists in two mechanically different phases, which are hereinafter referred to as Low-Density (LD) and High-Density (HD) C-S-H gels [42]. The paste's chemical composition is not absolutely constant but may differ a little from place to place, as well as porosity can. The hydrated cement consists of the inner product rich in high-density C-S-H gel, formed within the original boundaries of the cement grains (see Fig. 4.1), and outer product created mainly of low-density C-S-H gel mixed with other hydrates [43].

Unhydrated residues of Portland cement particles are found in almost all cement pastes and are easily identifiable. The clinker constituents are crystalline, with typical grain sizes ranging from about 1 µm to 60 µm. The clinkers are typically ground to a size of approximately 2 µm to 80 µm with a typical mean diameter of 20 µm to 40 µm [43]. Because the unhydrated components in cement have a much higher electron backscattering intensity than the hydrated products, these residual grains appear as bright clumps in (Scanning Electron Microscopy) SEM images (see Fig. 4.1, clinker).

In addition to the outer products, which appears darker in the SEM images than

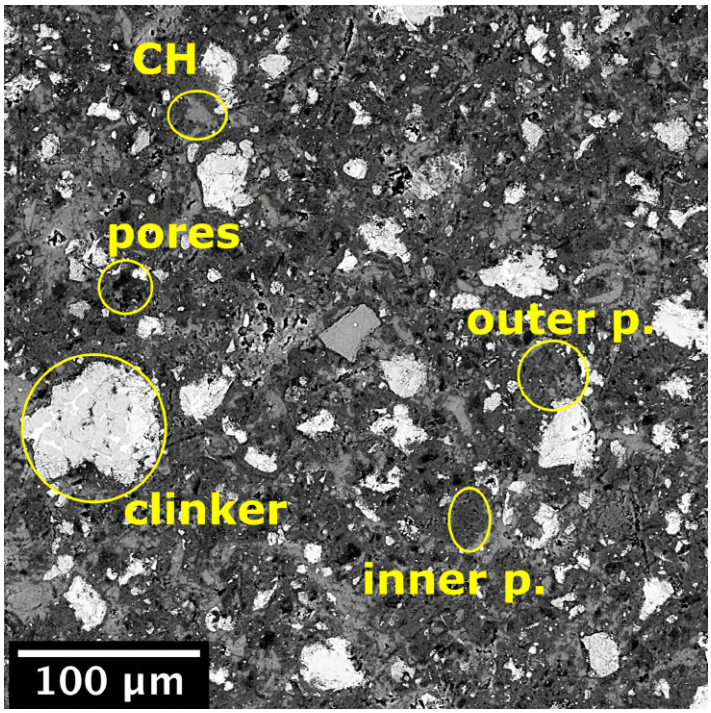

Figure 4.1: Individual phases of the ordinary cement paste showed on the SEM-BSE image.

the inner products, many individually distributed pores can be observed. These pores are represented in black in the image. There are several types of pores, which are described in more detail below. There are also large and irregular CH products (see Fig. 4.1), which have a slightly brighter appearance than C-S-H phases. Portlandite is formed as a by-product of the reaction of C_3S and C_2S with water [43].

Due to the European norm EN 197 [44] there are five classes of common cements where each class allows different limit of the weight of portland cement to be replaced. For first class CEM I it is allowed to replace up to 5% of weight of portland cement with other constituents and for second class CEM II it is allowed to replace up to 35% of portland cement with constituents that are permitted. Those are for example furnace slag, silica fume, fly ashes or other pozzolans. There are three other classes that allow even greater cement substitution.

4.1.1 Degree of Hydration

The hydration of the cement paste occurs at the moment when the cement comes into contact with water and continues theoretically infinitely. To describe the hydration of a cement paste, the Degree of Hydration (DoH) is used, which indicates the percentage of hydrated particles. The value of the degree of hydration ranges from 0 to 1, where 0 means that no cement particles have reacted and 1 means that all particles have reacted [45]. The Fig. 4.2 shows a comparison of the DoH in time model developed by Riding et al. (2013). Riding's model shows the effect of the water to cement (w/c) ratio on the overall DoH. It is obvious, that the hydration is different for various water to cement ratios [46].

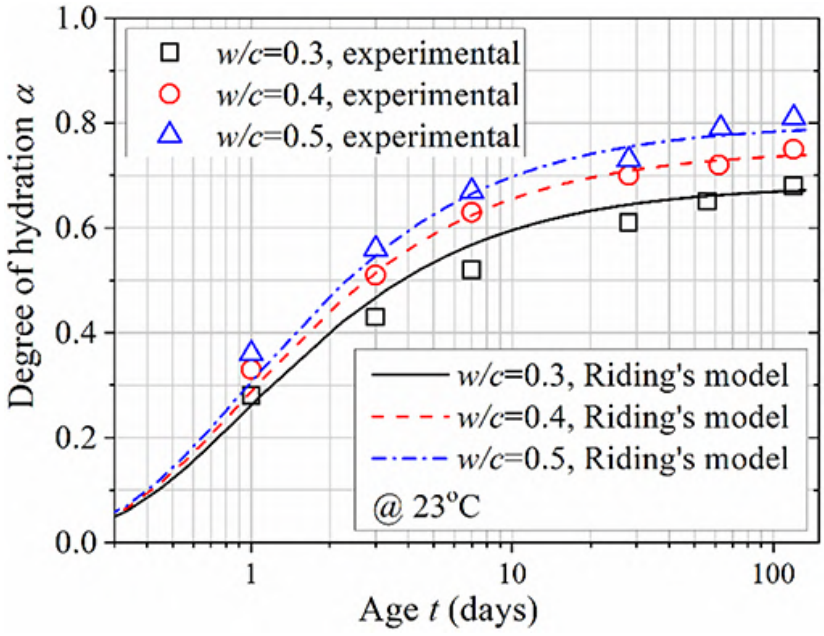

Figure 4.2: Comparison of DoH for different w/c ratios [46].

In 1948 T.C. Powers and T.L. Brownyards developed the first complex model of Portland cement hydration, which included unhydrated cement, capillary water, solid hydration porducts (CSH + CH), voids [47, 48].

While for the ratio w/c=0.3 it is evident that all the cement is hydrated, all the water is extracted from the capillary pores and a certain volume of solid hydration products is formed (see Fig. 4.3), for the ratio w/c=0.5 it is evident that even after complete hydration there is still water left in the capillary pores and a smaller volume of solid hydration products is formed, which results in a lower strength [50, 51].

The quantification of the individual microstructural phases for the determination of DoH can also be done experimentally using isothermal calorimetry [52] or by using computer models [53].

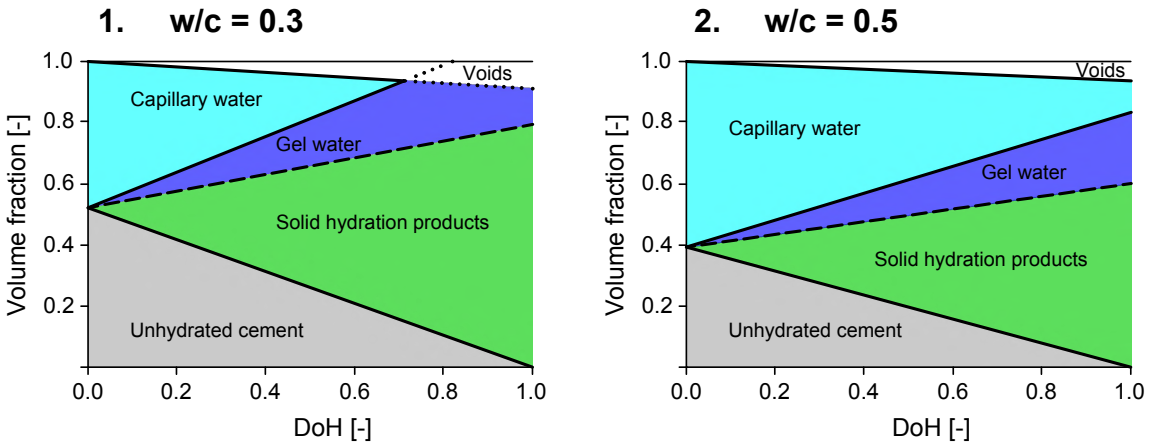

Figure 4.3: Transformation of individual components for different w/c ratios [49].

There are also more modern models for determining DoH, e.g. Cemhyd3D [54] or Hymostruc3D [55]. Cemhyd3D is a computer model that represents the microstructure by volume elements (cubic voxels). Individual phases such as anhydrous cement particles, pores or hydration products are represented by cubic voxels. The model includes chemical composition, curing conditions, particle size distribution and temperature. The behavior of the voxels is similar to that of real phases, including diffusion, dissolution, transport, and formation of the new hydration products. Particles are represented by the model as multiphase, irregular and multidimensional elements [56]. The Hymostruc3D treats all particles as interacting spheres and distributes them randomly. To make this simulation simple and realistic, periodic boundary conditions are used. Using the calculations, it is possible to know the composition of the hydration products at different curing ages and water/cement ratios. The Hymostruc3D model is influenced by the amount of water, the size distribution of the clinker particles and temperature [55].

4.1.2 Experimental techniques used for microscale investigation

ThermoGravimetric Analysis (TGA)

TGA is a method that captures the change in sample weight as a function of temperature. This method monitors the weight of a sample of the substance under investigation as its temperature changes. TGA characterizes and identifies phases from a complex cement matrix [57]. Similarly to (X-Ray Diffraction) XRD analysis, changes in the C-S-H phase, Portlandite, and calcite can be observed [58].

To interpret the results of the TGA analysis, it is necessary to process the TGA curves, see Fig. 4.4. In particular, the derivative of the TGA signal, represented by the (Derivative thermogravimetry) DTG curve, makes it possible to determine the

time point or temperature at which the fastest weight change occurs [57]. Hydrated cement exhibits significant mass losses up to a temperature of 200 °C, which are attributed to desorption of surface water, as well as water losses from C-S-H gel layers and dehydration of ettringite. Further weight loss up to about 400 °C indicates thermal decomposition of hydrated silicate and aluminate type compounds. Further, the thermal decomposition of Portlandite takes place, followed by the decomposition of carbonate phases (only for carbonated concrete) and calcite. The temperature range during the experiment is usually between 30 °C and 1000 °C [21].

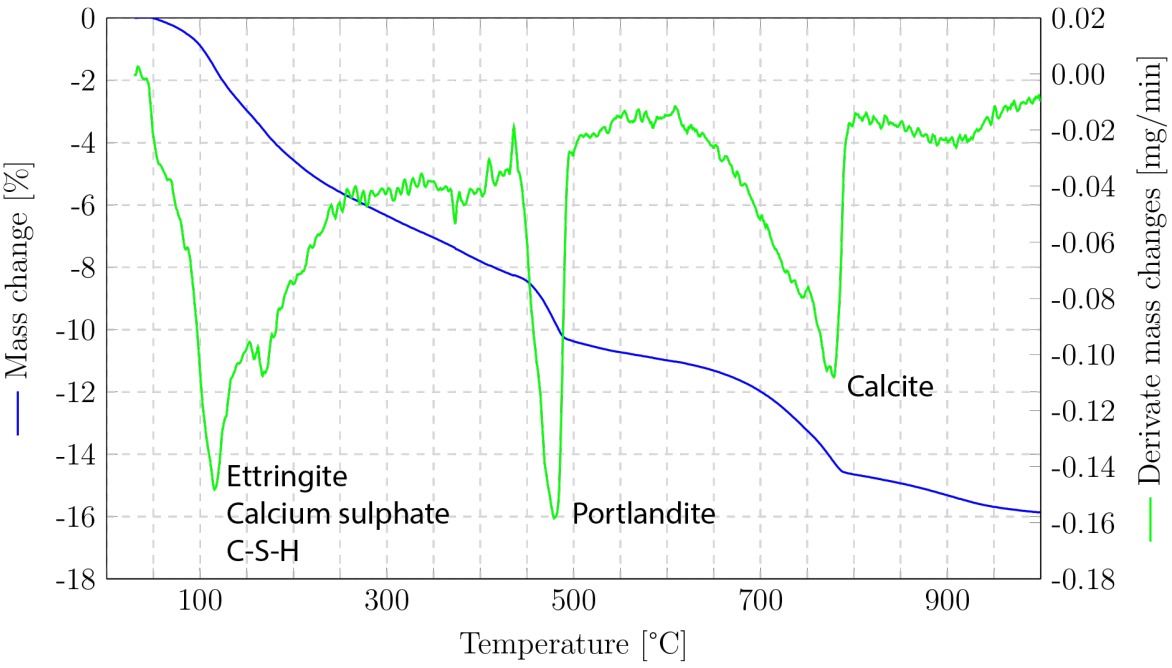

Figure 4.4: TGA and DTG curves of concrete.

Decomposition of the cement paste can be described using following Eq. 4.3-4.5 [59–61]. Dehydration of calcium silicate hydrate (C-S-H):

$$x\text{CaO}.y\text{SiO}_2.zH_2O \longrightarrow x\text{CaO}.y\text{SiO}_2 + z\text{H}_2\text{O}, \tag{4.3}$$

where x, y, z represent the stoichiometric coefficients of the C-S-H gel.
Dehydroxylation of calcium hydroxide:

$$\text{Ca(OH)}_2 \longrightarrow \text{CaO} + \text{H}_2\text{O}. \tag{4.4}$$

Decomposition of calcium carbonate:

$$\text{CaCO}_3 \longrightarrow \text{CaO} + \text{H}_2\text{O}. \tag{4.5}$$

X-Ray Diffraction (XRD)

XRD is a technique that provides chemical information for elemental analysis as well as for phase analysis. Samples to be analyzed using XRD must be crystalline as concrete samples partly are [62]. XRD analysis is used to show cement microstructure's phases such as Portlandite, Calcite, clinker, AFm, and AFt, where the microstructure changes of a cement matrix are expected during current application [58].

From the measurement of the intensity of the scattered waves as a function of the scattering angle, a diffraction pattern is obtained where Bragg peaks can be observed. The atomic structure of crystals can be determined from the data obtained from the interference of X-rays passing through a crystal [63]. The XRD analysis output is shown in Fig. 4.5.

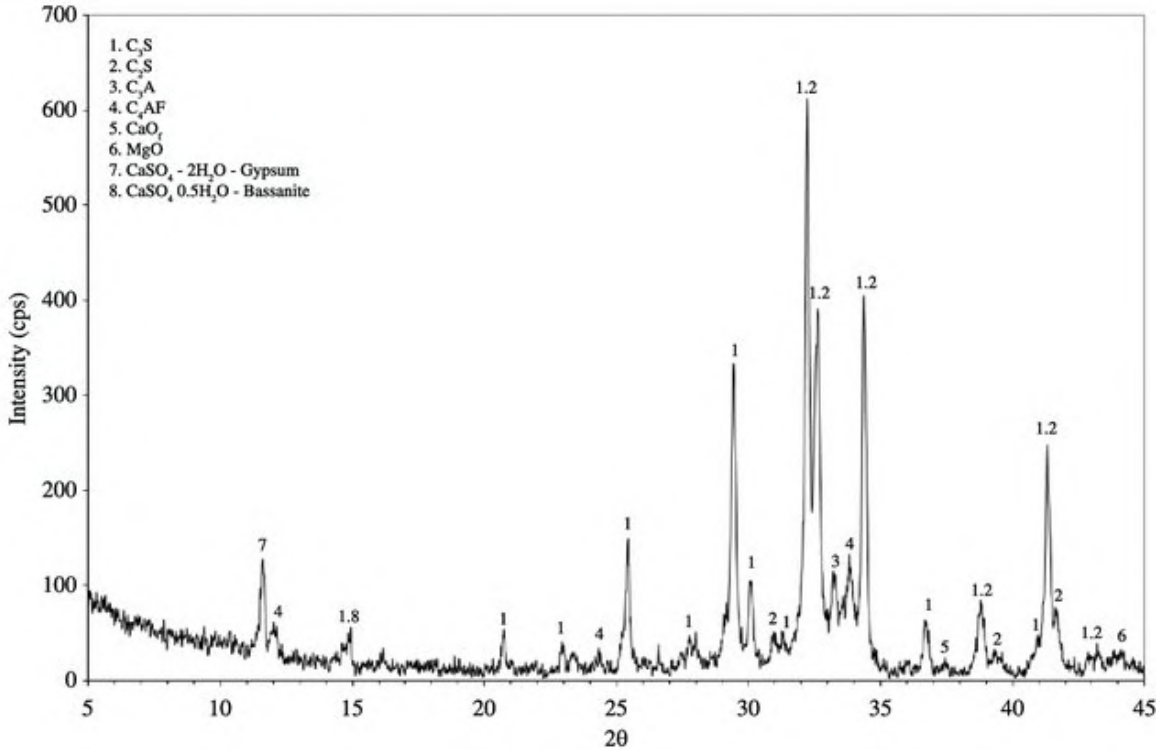

Figure 4.5: The X-ray diffraction of the cement CEM I 42.5N [64].

Scanning Electron Microscopy (SEM)

SEM is a type of microscopy that provides images of samples by scanning their surface in interaction with a beam of electrons. The electrons interact with the atoms in the sample and produce various signals that contain information about the surface topography and composition of the sample [65]. Back-scattered electrons (BSE) detectors are commonly integrated into SEM instruments. They are generally placed above the sample in a chamber based on the scattering geometry with respect to the incident beam. BSE detectors are semiconductor devices, often with separate components to simultaneously collect backscattered electrons in different directions. Detectors above

the sample collect backscattered electrons as a function of sample composition, while detectors located on the side collect backscattered electrons as a function of surface topography [65]. Another type of signal, such as (SE), are the main means of viewing morphology. SEM coupled with energy dispersive spectroscopy (EDS) has many applications in cement composites. In particular, it provides elemental composition analysis (see Figs. 4.1, 4.6). The basic prerequisites for conventional quantitative analysis are: uniformly polished surface, homogeneous composition in the analytical volume, stability of the sample under the electron beam, etc. High-quality quantitative analysis of hydrated cements is somewhat problematic, precisely because of violations of these assumptions.

Image analysis

Image analysis is a mathematical tool used for post-processing of SEM images of cement paste phases. The observed parameters are e.g. the size of the phases, their representation, and shape. Images are captured in a gray range (0-255) of colors, and the colors of pixels vary according to the density of the physical element. The darker colored pixel in the SEM-BSE image represents elements with a lower proton number, while the lighter colored pixel, on the other hand, represents areas with elements with a higher proton number [66]. The result of image analysis is a colored image, where each color represents a specific material phase separated by a given threshold. From this it is possible to determine the percentage representation of the individual colors, see Fig. 4.1.

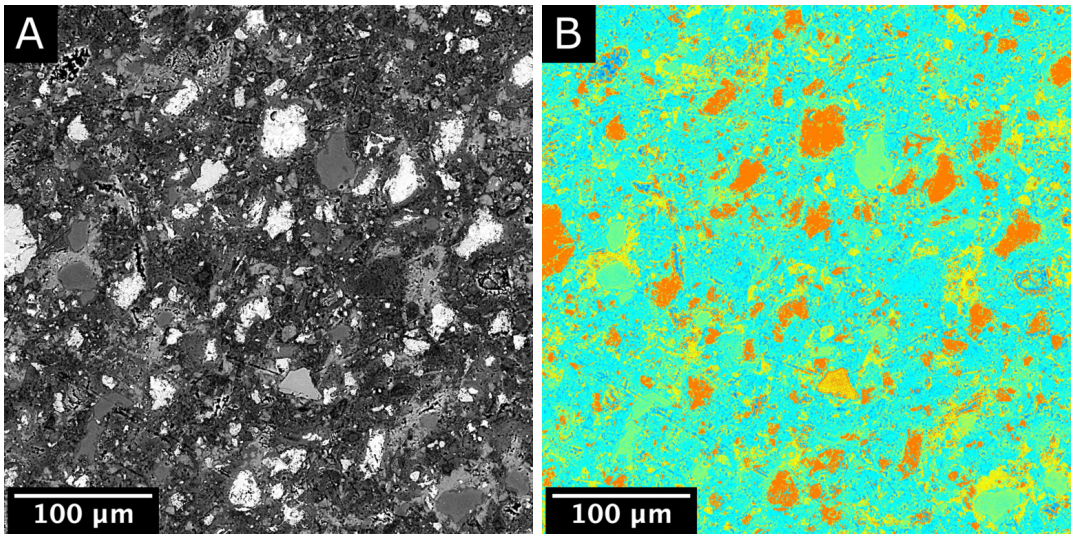

Figure 4.6: A) SEM-BSE photo B) marked phases after image analysis, where blue color represents pores, yellow portlandite, orange clinker, green HD C-S-H and turquoise LD C-S-H.

During the image analysis, adequate gray-level threshold assessment is necessary. Otsu method can perform automatic image thresholding, whose algorithm in its sim-

plest form returns a single intensity threshold that separates pixels into two classes [67]. It is important to select an adequate gray-level threshold for extracting individual objects when processing an image. Various techniques have been proposed in this regard. Ideally, the histogram (see Fig. 4.7) has a deep and sharp valley between two peaks representing objects, so choosing a threshold at the bottom of this valley is possible. However, it is often difficult for most images to accurately detect the bottom of a valley, especially when the valley is flat and wide, full of noise, or when the two peaks are extremely different in height and often without creating a detectable valley. In computer vision and image processing, the Otsu method is used to perform automatic image thresholding, whose algorithm in its simplest form returns a single intensity threshold that separates pixels into two classes. Using this method, pixels can be separated into several classes. In this method, the image is viewed as two groups of points with different ranges of intensity values. The problem is that these intensity ranges usually overlap, and therefore the method seeks to minimize misidentification of pixels [67].

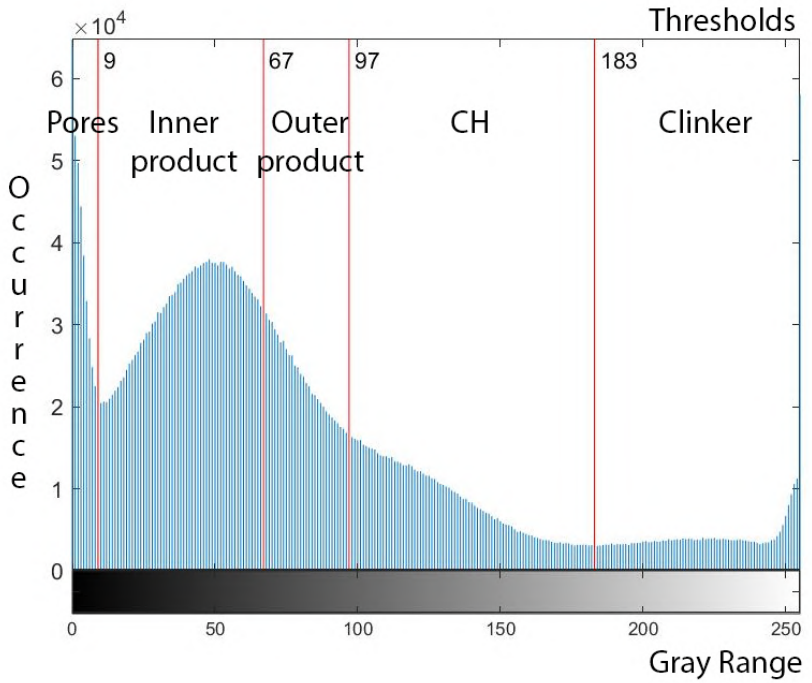

Figure 4.7: Histogram representation of individual gray ranges with thresholds determined by the Otsu method.

4.1.3 Porosity

The cement hydration reaction produces a solid and a pore system. Therefore, porosity is inherent in concrete. Porosity in concrete can also be caused by insufficient compaction. The characteristics of the matured cement are also determined by the characteristics of the pores, which differ in shape, size and distribution in the solid matrix. This pore system determines the most important properties of concrete, especially its strength [68]. Chloride diffusivity is strongly influenced by the pore size distribution, shape and pore connectivity. Generally, higher porosity allows chlorides to travel easier through the porous system [69, 70].

4.1.4 Pore types

The pore system in concrete constists of a continuous spectrum of pores that can be roughly categorized to the three types:

- Gel pores (0.5 - 10 nm),
- Capillary pores (10 - 10 000 nm),
- Micro and macro pores (> 10 000 nm).

In addition, air voids can be formed [71, 72].

The first type are gel pores with the smallest nanopores with characteristic dimension 0.5 - 10 nm located in the C-S-H gels. Despite their small dimensions the gel pores are the biggest cause for the shrinkage and the creep. The water present in the gel pores does not evaporate under ordinary conditions. The water absorbed in the interlayer space, which is part of the gel pores with size less than 0.5 nm, is not liquid but chemically bound and therefore cannot be removed by drying [34].

The second type are capillary pores of average radius dimensions from 10 to 10000 nm located in the mix water formerly occupied space and surrounded by LD C-S-H gels. The water in capillary pores is evaporable. As the volume of capillary pores increases, the strength of the concrete decreases [73].

The third type are the micro and macropores from intentionally entrained air and from insufficient compaction with average pore radius from 10000 nm. As a result of the process of shrinkage, mechanical stresses and as a result of tensile stresses developed by hydration heat in solid structures, the cracks are formed. Air voids are caused by imperfect placement or concrete mixing technology and have range from micrometers [34].

4.1.5 Experimental techniques for pore description

Several methods are generally used to measure the porous structure of concrete, such as the open porosity (OP) measurement, image analysis of SEM or light microscope images, Mercury Intrusion Porosimetry (MIP), gas pycnometry, proton nuclear magnetic resonance (^{1}H-NMR), and electrochemical impedance spectroscopy (EIS). An approximate validity range of the methods are shown in Fig. 4.8 with the pore diameter range that can be observed with them [74].

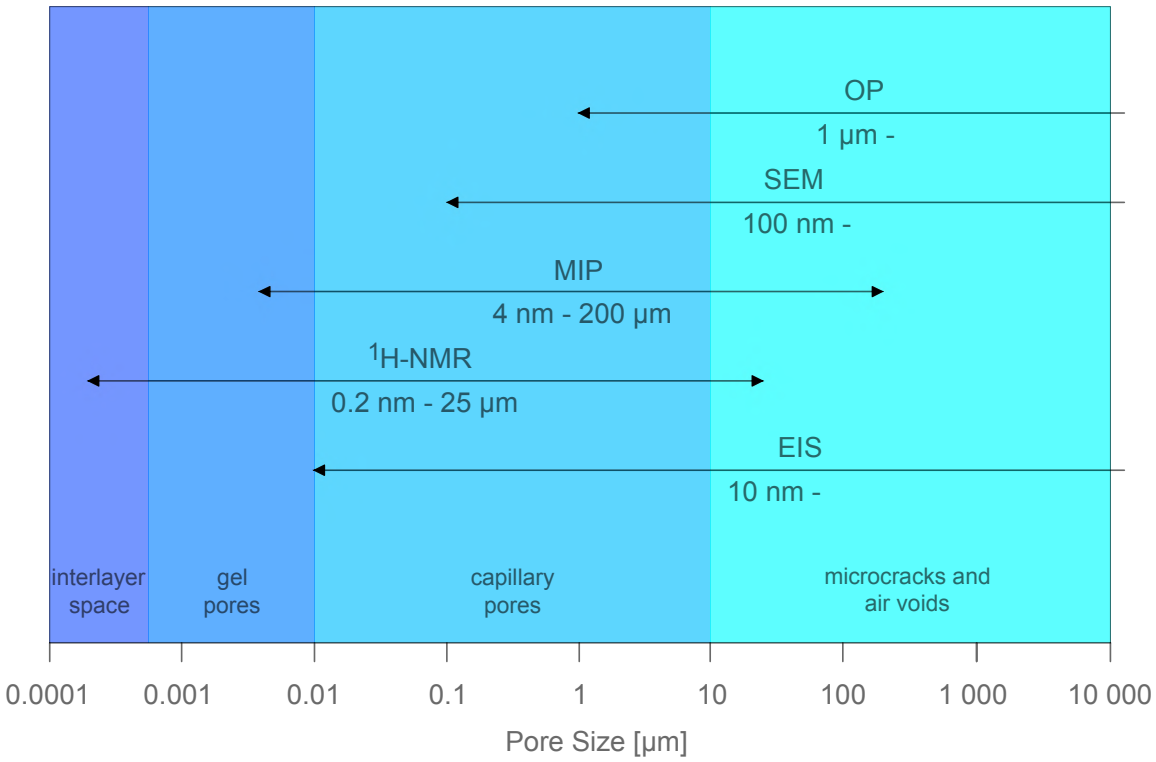

Figure 4.8: Approximate validity of methods used to determine porosity and pore size distribution [74].

Open Porosity (OP)

The OP measures the evaporable water from the pores. Its weight is needed to determine the total open porosity. The open porosity, ϕ_{OP} is then calculated according to the equation:

$$\phi_{\mathrm{OP}} = \frac{V_{\mathrm{w}}}{V_{\mathrm{s}}} = \frac{m_{\mathrm{w}} - m_{\mathrm{d}}}{V_{\mathrm{s}}.\rho_{\mathrm{w}}}, \tag{4.6}$$

where V_{w} is a volume of the evaporable water, V_{s} is a volume of the concrete sample, m_{w} is a weight of fully saturated sample. m_{d} is a weight of dried sample and ρ_{w} is a density of water assumed as 998 kg/m^3 at 20 °C.

Mercury Intrusion Porosimetry (MIP)

MIP has been used for many years to investigate the porous structure of cement-based materials. MIP also provides information about the connectivity of the pores [75]. Measurement of porosity by mercury intrusion provides an extensive range of measurable pore sizes from 4 nm to 200 µm. However, it is important to note that mercury intrusion porosimetry only measures the open pores [76].

The standard MIP measurement is performed as follows. The samples are first dried to remove water from the pores. The dried samples are weighed and placed in a chamber. Air is evacuated from the chamber, causing the air to be removed from the sample. The chamber is then filled with mercury (see Fig. 4.9) where it is then forced into the sample by the applied pressure. The volume of mercury intrusion and the corresponding applied pressures are recorded during all pressure steps [77]. For measuring small pores a high pressure needs to be applied, which can damage the microstructure of the material.

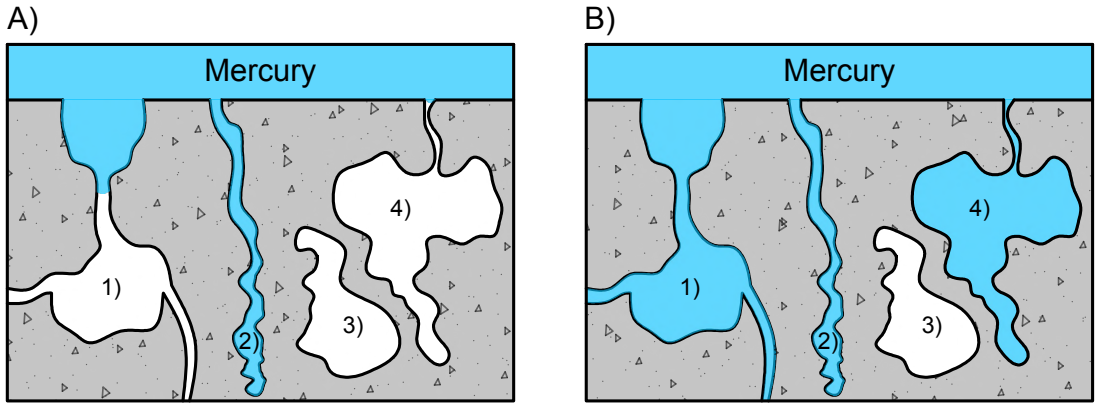

Figure 4.9: Mercury intrussion into a cement paste using A) low pressure and B) high pressure. Accessibility of 1) pores accessible through the small opening, 2) capillary pores, 3) inaccessible closed pores, 4) Ink-bottle pore with throat pore opening [78].

From the measured pressure the pore size can be calculated then using Washburn's equation [79]:

$$d_{\mathrm{p}} = -\frac{4.\gamma.cos\theta}{p}, \tag{4.7}$$

where d_{p} is the cylindrical considered pore radius, γ is the surface tension, θ is the contact angle and p is an imposed pressure, where γ and θ are assumed as constant [79].

The result obtained from MIP include the pore size and the pore volume distribution. Summary providing measurements of total intrusion volume of Hg (ml/g), volume median pore diameter (µm), total pore area (m^2/g), bulk density (ml/g), skele-

tal density (ml/g) and porosity (%). The results can be then processed into a graph (see Fig. 4.10).

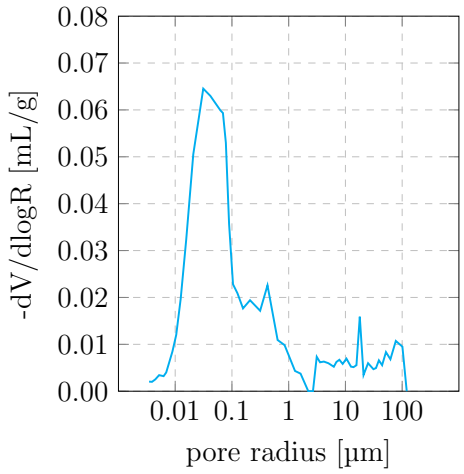

Figure 4.10: Pore volume distribution obtained from MIP measurement of concrete sample.

^{1}H-NMR

Nuclear Magnetic Resonance (NMR) with focus on ^{1}H protons is non-destructive method which can be also used to observe porosity of the cementitious materials. The NMR method involves the interaction of atomic nuclei with a magnetic field and can be divided into low-resolution and high-resolution applications. The high resolution application is also known as spectroscopy. It allows the analysis of structural information on a molecular basis and the analysis of chemical properties. The method is not suitable for the observation of larger types of samples because the weight of the sample is usually limited to a few grams. For larger sample types, or for on-site structural applications, a low-resolution NMR application that includes relaxometry and diffusometry measurements is preferable. It is known as dynamic NMR and provides information e.g. on fluid transport and structure cf. It is used to determine the permeability, porosity and water content of, e.g., cement-based composite materials [80].

Electrochemical impedance spectroscopy (EIS)

EIS method can be used to observe resistance of materials like concrete and cement paste as a non-destructive method [81]. Resistance is measured using a pair of electrodes mounted on opposing surfaces or embedded in the material to which an alternating current (AC) is applied. The recorded parameter is impedance. The use of the EIS in cementitious materials allows the detection of several processes, including the hydration and shrinkage processes, chloride diffusion in concrete, porosity, microstructure or corrosion processes [82, 83].

4.2 Chloride transport

Chloride ions can penetrate concrete through various mechanisms, ultimately reaching the steel reinforcement and initiating the corrosion process. Chloride transport in concrete includes several basic physio-chemical mechanisms such as diffusion of chloride ions in the pore solution and physical and chemical interactions between the ions and the pore surfaces [18–20, 84, 85]. Other mechanisms include migration in an electric field, absorption due to capillary action or pressure-induced flow [86].

4.2.1 Chloride transport mechanisms

The main mechanisms of chloride transport are:

- Capillary Absorption: When concrete is exposed to a chloride-containing solution, the liquid penetrates the capillary pores in the cement paste. This action is driven by the surface tension of the liquid and the attraction between the liquid and the pore walls. The chloride ions present in the solution are transported into the concrete matrix. Capillary absorption is more pronounced in concrete with a higher water to cement ratio [28].
- Hydrostatic Pressure: Chloride penetration by hydrostatic pressure occurs when the concrete structure is submerged or partially submerged in water containing chlorides. The pressure difference between the water and the interior of the concrete forces chloride ions to penetrate the concrete matrix. This mechanism is particularly important in underwater structures such as bridge piers and marine installations [29, 30].
- Diffusion: During diffusion, chloride ions move from areas of higher concentration to areas of lower concentration. In concrete this occurs through the porous system in the cement paste. This process is described by Fick's diffusion laws and is influenced by factors such as concrete porosity, chloride concentration gradient, temperature and humidity. Diffusion is the main mechanism of chloride transport in saturated or partially saturated concrete where capillary absorption is limited [5, 26, 27].

Fick's first law describes the relationship between the flux of chloride ions and the concentration gradient within the concrete matrix:

$$J = -D.\frac{dC}{dt}, \tag{4.8}$$

where J is the flux of chloride ions, D is the diffusion coefficient of chloride ions, and $\frac{dC}{dt}$ is the concentration gradient of chloride ions [5].

Fick's second law describes how the concentration of chloride ions C changes with time t and space x within the concrete matrix

$$\frac{dC}{dt} = D.\frac{d^2C}{dx^2}, \tag{4.9}$$

where $\frac{dC}{dt}$ is the rate of change of chloride ion concentration with time, D is the diffusion coefficient of chloride ions in concrete [5, 27].

The solution of the Eq. 4.9 equation in 1-D with Dirichlet b.c. leads to:

$$C(x,t) = C_{\mathrm{s}}\left[1 - erf\left(\frac{x}{2\sqrt{Dt}}\right)\right], \tag{4.10}$$

where C_s [wt.%] is a surface chloride concentration, D [m^2/s] is diffusion coefficient, t is time and $C(x,t)$ is concentration of chloride after time t in x depth [87].

Chlorides, as charged particles, can also be transported by an external electric field that affects their charge and allows them to move in a given direction. Electrochemical transport is a process in which ions move due to a combination of a concentration gradient and an electric field. In such cases, Fick's laws are not sufficient because they do not account for the electrical forces acting on the ions. Instead, the Nernst-Planck equation is used. The Nernst-Planck equation can be in one dimensional case written as:

$$\frac{dC}{dt} = D.\left(\frac{d^2C}{dx^2} + \frac{zF}{RT}.\frac{dC}{dx}.\frac{d\Phi}{dx}\right), \tag{4.11}$$

where z is the ion valence, F is the Faraday's constant, R is the universal gas constant, T is the temperature and Φ is the applied electrical potential [5].

4.2.2 Chloride binding

The ability of concrete to bind chloride depends on factors such as the type and quantity of cementitious materials, the ratio of water to cement, the age of the concrete and the environmental conditions [19, 88–90]. The basic mechanisms of chloride binding can be summarized as:

- Physical adsorption: Chloride ions are attracted to the surface of cementitious materials by weak electrostatic forces and thus physical absorption occurs. Absorption occurs primarily in C-S-H gels and pore walls in the cement matrix. Physical absorption is considered to be a major contributor to chloride binding. However, when the concentration of free chloride ions decreases, the physical absorption of chloride on the surface of the C-S-H gel decreases, which means that physical absorption is a reversible process [91, 92].

- Chemical binding: Chemical binding describes the reaction of chloride ions with the hydration products of cement to form stable or semi-stable chloride-containing compounds. The main mechanism of chemical binding is Friedel's salt formation, where chloride ions react with the aluminate phases of the hydrated cement (mainly monosulfate and AFm phases) to form Friedel's salt. Friedel's salt is a stable compound that immobilizes the chlorides, thereby reducing their availability for rebar corrosion [92].

- Physical entrapment: This process is not a binding mechanism, but contributes to the reduction of chloride concentration. Chloride ions can be physically trapped in the capillary pore structure and diffusion of chloride ions can be slowed down due to the difficult pathway that the ions must pass through.

For chlorides in concrete, a distinction is made between free and bound chlorides, an equilibrium is established between the two. The adsorption isotherm method was chosen to characterize chloride incorporation in the test material. The process is based on bringing concrete powder into equilibrium after placing it in a chloride-containing solution. The initial concentration of chloride in the solution decreases due to chloride adsorption in the concrete, and from this difference in concentration, the amount of chloride bound in the sample can be determined. Similarly, desorption experiments can then be performed to monitor the amount of chloride leached back into solution [19].

It was also shown, that the chloride ion binding capacity of ordinary portland cement (OPC) concrete largely depends on the C-S-H gel content in the concrete, independent of the water-cement ratio and the addition of aggregates. The relationship between bound and free chloride is well described by chloride binding isotherm [19, 88, 89]:

- Freundlich isotherm: The Freundlich isotherm is an empirical model that describes the non-linear relationship between the concentration of free chloride ions in the pore solution and the concentration of bound chloride ions in the solid phase. The Freundlich isotherm can be applied to chloride binding in concrete, considering the variability and heterogeneity of cementitious materials. However, it may not be suitable for predicting binding behaviour low chloride concentrations (<0.01 mol/l) [19].

- Langmuir isotherm: The Langmuir isotherm is a model that assumes monolayer adsorption on a homogeneous surface with a fixed number of adsorption sites. The Langmuir isotherm is more appropriate for systems with a well-defined and homogeneous surface and for low (<0.05 mol/l) free chloride concentrations [19].

4.2.3 Corrosion of reinforcement

Concrete is a highly alkaline environment with pH value between 12 and 14. Within this alkalinity range, the concrete reinforcement is protected from corrosion by a passivization film bonded to the reinforcement surface. It is called alkaline passivization of the reinforcement by the concrete. However, when the passivization film breaks down, corrosion of the reinforcement can occur.

Reinforcement corrosion is an electrochemical process that needs an anode, a cathode and an electrolyte. Moisture in the concrete forms a suitable electrolyte and the steel reinforcement forms the anode and cathode. An electric current is passed between the anode and cathode and the reaction results in an increase in the volume of metal in the structure as Fe (iron) oxidizes to $Fe(OH)_2$ (rust). Water and oxygen must be present for the reaction to proceed [22]:

$$2Fe + O_2 + 2H_2O \longrightarrow 2Fe(OH)_2 \tag{4.12}$$

Further corrosion then produces higher oxides, not only $Fe(OH)_2$. The volume per mass unit of typical rust is approximately 2 to 14 times higher than the volume of steel. This expansion causes cracking and spalling of the concrete cover. As the corrosion process continues, the steel can lose its structural integrity, which can lead to failure of the reinforced concrete structure. The exact volume change depends on the specific reaction conditions and the extent of corrosion [22].

4.2.4 Chloride transport in cracked concrete

The presence of chlorides in concrete structures itself might not be so problematic if it were not for its porous system, through which chlorides travel. The problem is also the cracks that form on the surface of the concrete, they open up and travel to the reinforcement, thus allowing chlorides to pass through. The chlorides then travel to the reinforcement, where they cause corrosion, which is one of the biggest problems of reinforced concrete structures and it is then the main cause of loss of properties of reinforced concrete structures [18–20].

Several studies have shown that the presence and size of cracks can significantly increase the rate of chloride sulphation into concrete and thus the rate of steel corrosion. For example, studies have shown [23–25] that the corrosion rate of reinforcing bars in the concrete with cracks is significantly higher than in concrete without cracks.

Various studies [93, 94] have found that the effective diffusion coefficient of chloride ions in concrete with cracks is significantly higher than in concrete without cracks. In addition to the increase due to cracks, it has been found [95] that exposure to high temperatures can also increase the effective diffusion coefficient of chloride ions.

4.2.5 Ionic Mobility

The ability of concrete to resist is also influenced by the movement of ions in its cement matrix. The mobility of ions plays an important role in determining the transport properties of the concrete, such as electrical conductivity, permeability and chemical reactivity [96, 97]. The ion mobility of OH^- and Cl^- ions is of particular interest in this thesis. The mobility of OH^- ions is approximately 2.5 times higher than that of Cl^- ions [98, 99].

A various experimental methods are available for the evaluation ionic mobility in the concrete. One of the methods is the ion migration test, in which an electric field is applied to a concrete sample measuring the movement of ions in the pore solution. Another method is, e.g. rapid chloride permeability test, evaluating the rate at which chloride ions penetrate a concrete sample under specific conditions. Electrical resistivity measurements also offer a measure of the mobility of ions in concrete [100]. A widely-used standard for performing the ion migration test is the NT BUILD 492 (Nordtest Method) or the equivalent European Standard EN 12390-16:2019 "Testing hardened concrete - Part 16: Determination of the chloride migration coefficient in hardened concrete using a non-steady-state migration experiment.". The test mainly focuses on chloride ions (Cl^-), as these are the most common cause of reinforcement corrosion in concrete structures. However, the testing method can also be adapted to evaluate the migration of other ions, such as sulfate ions (SO_4^{2-}), carbonate ions (CO_3^{2-}), or other species of interest, by modifying the test setup and solution compositions.

4.2.6 Non-accelerated tests

The ponding (diffusion) test is one of the methods measuring the penetration of chlorides into the concrete. A considerable time is required for chloride ions to penetrate into the concrete sample. Usually, all sides except one are covered with acrylic, which ensures that the transport of chlorides is uni-directional. The samples are usually subjected to 3-10% NaCl solutions for 28-365 days. The result of the test is a chloride profile that can be compared with other experimental methods [27].

4.2.7 Determination of chloride concentration

In order to determine the chloride concentration, it is necessary to prepare the sample to be tested in advance. This is usually done as follows [101]:

- Layer grinding: Removal of the concrete layers at different depths at predetermined intervals (e.g. every 5 mm or 10 mm). The concrete powder from each layer is placed in the containers for further analysis, and the depth of each layer is recorded.

- Sample preparation: The weighed concrete powder is mixed with a certain volume of deionised water. Chloride extraction is then carried out from the solid sample, after which the liquid phase containing the extracted free chlorides is filtered off from the solid residue. When testing the total chloride content of concrete, including both free and bound chlorides, the acid extraction method is usually used. In this case nitric acid (HNO_3) is used, typically at a concentration between 0.5 M and 2 M. The same acid was also used to process the samples used in this thesis.

The prepared sample can be examined using any of the following methods [19, 101, 102]:

- Potentiometric titration: The liquid phase obtained from the sample preparation is titrated with silver nitrate ($AgNO_3$) solution of known concentration. A silver/silver chloride (Ag/AgCl) electrode is used to measure the change in potential during titration. The final point of the titration is determined by an abruptly change in potential indicating the completion of the reaction of the chloride with the silver. By measuring the amount of $AgNO_3$ solution used, the chloride content can be calculated. Potentiometric titration was used in this thesis.

- Ion-selective electrode (ISE) probes: Instead of potentiometric titration, the ISE probe can be used to directly measure the chloride concentration in the liquid phase. The ISE chloride probe is highly sensitive to chloride ions and uses a reference electrode to measure the electrode potential.

Based on the results, the chloride content is calculated for each layer of the sample, the data analysis is processed and a chloride profile is produced [101].

4.2.8 Accelerated electric tests

Rapid Chloride Permeability Test (RCPT)

There are several standardized accelerated tests for chloride penetration to concrete. One of them, the RCPT measures the electric charge transferred through concretes from which it is possible to determine their resistance to chloride ion penetration on various mixtures. The test is carried out by monitoring the amount of electric current that passes through the concrete samples in a specified time. The standard test according to AST C1202 consist of cylindrical 50 mm thick slices with a diameter of 100 mm. The concrete samples are exposed to a potential difference of 60 V direct current for 6 hours, where electric current passing through samples is monitored [9]. In the chambers there is the negative pole in 0.52 M NaCl solution and positive pole in 0.30 M NaOH solution which are in contact with sample's base.

The RCPT results are classified into five categories based on the charge passed through the concrete sample during the test:

- High chloride ion permeability: The charge passed through the concrete sample is greater than 4000 C. These types of concrete are more susceptible to chloride-induced corrosion.
- Moderate chloride ion permeability: The charge passed through the concrete sample is between 2000 and 4000 C. These types of concrete are not as susceptible to chloride-induced corrosion as high penetrability concrete, but still requires attention in aggressive environments.
- Low chloride ion permeability: The charge passed through the concrete sample is between 1000 and 2000 C. This level of permeability indicates a relatively low risk of chloride-induced corrosion.
- Very low chloride ion permeability: The charge passed through the concrete sample is between 100 and 1000 C. This level of permeability indicates excellent resistance to chloride-induced corrosion.
- Negligible chloride ion permeability: The charge passed through the concrete sample is smaller than 100 C.

The results of the test can be used to compare the permeability of different concrete mixtures. However, in order to classify, for example, alkali-activated concrete, it is necessary to compare the results of the electrical tests with the diffusion coefficients of chlorides, because this classification does not define all possible concrete mixtures. [103].

Electrochemical Chloride Extraction (ECE)

Another of the electrically accelerated tests is electrochemical chloride extraction, also known as desalination. ECE is a non-destructive and effective technique in chloride removal with extraction up to 70% of total chlorides [104].

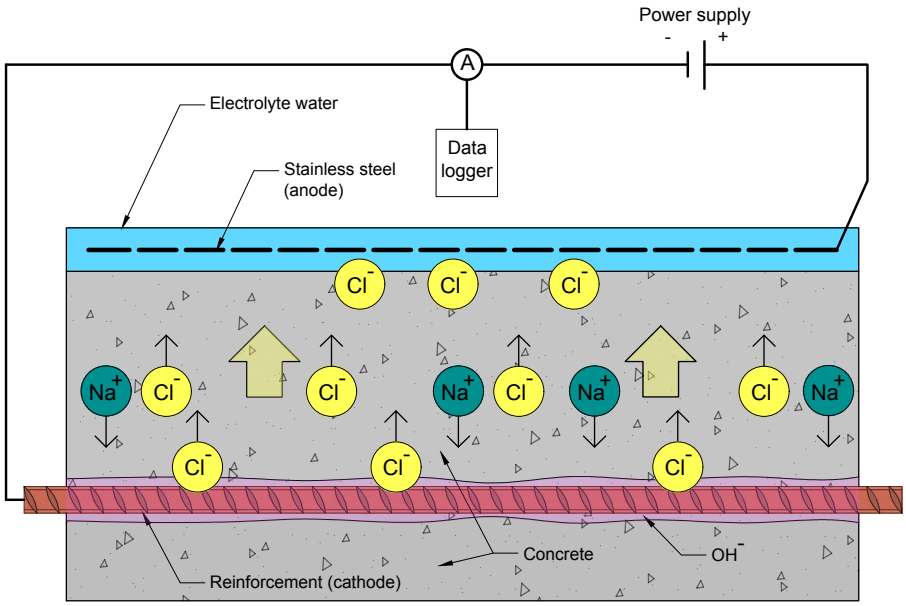

Figure 4.11: Scheme of the ECE test [105].

Between metal mesh fixed to the surface of the sample (anode) and reinforcement (cathode) there is an electric field [35]. While negatively charged cations (Cl^-, OH^-, etc.) are attracted to the anode, cations (Na^+, K^+, etc.) are attracted to the reinforcement's surface where hydroxyl ions (OH^-) are being produced, see Fig. 4.11.

Nanosilica injection

Injection of NanoSilica (NS) into the concrete is a technique improving the mechanical properties and durability of concrete structures. The principle of technique is injecting a nanosilica particles solution into the porous system of the concrete, where the particles then react with the cement matrix and form a denser and stronger material [33, 37, 38].

The most impressive properties of nanosilica are its high surface-to-volume ratio and high reactivity, which is exploited when an electric current is applied to generate an electric magnetic field that transports the particles from one pole to another through the sample. It is also properties such as good bonding ability with other materials or high pozzolanic activity which allow reaction with cement to produce additional C-S-H [33, 37]:

$$Ca(OH)_2 + \text{nano-}SiO_2 \longrightarrow CSH \tag{4.13}$$

The nanosilica particles were shown to be capable of blocking the subsequent penetration of chloride, and the nanosilica treated samples showed a reduction in chloride concentration on the surface of more than 70%. Based on this, it is estimated that nanosilica is mainly used to fill small capillary pores inside the sample [33].

4.2.9 Effect of electric current on porosity of concrete

Understanding the basic electrochemical properties and processes that occur to concrete when an electric current is applied allow to evaluate how those factors affect changes in the porosity. Factors influencing the porosity of concrete after current application are for example:

- Electro-osmotic Effects: This phenomenon changes the porosity temporarily. Although it induces electroosmotic movement of water in the saturated concrete, when the current is cut off the water is returned to the pores and the original porosity is restored [31, 32].
- Electrophoretic Migration: The ions move and interact with the hydration products in response to the electric current, which can cause dissolution of the hydration products and increasing porosity [36].
- Heating Effects: The electric current generates heat which induces thermal expansion of the concrete, which can lead to the formation of microcracks and increased porosity. When the electric current is removed, cooling occurs, which causes contraction of the material and may affect the microstructure of the pores and the overall porosity [34].

It was shown, that the process of electrochemical chloride penetration and electrochemical chloride extraction increases overall porosity. The 5% increase of porosity was measured in samples with ratio w/c = 0.35 after injection of the chlorides and about 16% increase in porosity was detected after the ECE test. In the samples with w/c= 0.55 ratio the increase in porosity was 10% after the injection and up to 22% after the ECE. For Ordinary Portland Cement (OPC) samples the highest initial porosity was measured after both electrochemical tests, but on the other hand the increase in porosity was smaller than for samples containing fly ash or slag, where an increase in porosity of up to 71% was recorded [104]. However, for example, this study [13] shows that the porosity can also decrease after the application of an electric current, since the change in porosity depends on the current density and the surrounding conditions.

5 Experimental part

The purpose of the experiment was to determine efficiency of individual treatments and the effect of electric current on the microstructure. Different mixtures of concretes and mortars were made to observe the changes during the different experiments. To observe and find the effect of experimental protocols, for example, some samples were exposed to chlorides either naturally or by electromigration techniques, etc. Specifically, the experiment was divided into four sets.

1. The samples in the first set were naturally exposed to chloride. Subsequently, the samples were divided into the two groups where one group of samples was subjected to natural diffusion in order do evaluate effective diffusion coefficient. The second group of the samples was subjected to chloride extraction using an electric current. This set was designed to determine the effectiveness of the extraction technique and also to observe porosity changes.

2. The samples in the second set were subjected to the electromigration test on samples submerged in NaOH solution, so the samples were saturated after test and then exposed to chloride in its natural form, i.e. placed in solution. This set determines whether the saturation by chloride in its natural form after the current is applied is different from the first set where the sample is exposed to chloride without prior electrical testing.

3. The third set of samples was designed to determine microstructural changes due to electrical treatments. The purpose was to determine the change in open porosity before and after the electrical test. For this set, analyses such as SEM, TGA, XRD were also performed to further refine the changes in the microstructure caused by the electric current. Subsequently, the samples were subjected to electric chloride penetration, which provided data to compare natural chloride diffusion and accelerated penetration. The data obtained were also compared with the fourth set.

4. In the fourth set, all samples were injected with an electric current using nanosilica. The samples were then exposed to chlorides. One part of the samples was exposed to natural diffusion and the other to accelerated chloride penetration. The results were compared with the other sets. The aim was to check whether the injection of the nanosilica actually has any effect on the chloride resistance and whether the microstructure is affected by the nanosilica injection.

5.1 Sample preparation

Concrete and mortar samples in the shape of a cylinder with a base diameter of 100 mm and a height of 200 mm were prepared. From this cylinder, 25 mm of the top and bottom were then cut and the remaining 150 mm were divided into 3 samples of 50 mm height. This procedure was carried out for all concrete and mortar mixtures. The hydration time of the individual samples is shown in Fig. 5.3. Since the microstructure and thus the porosity of mortar is different from that of concrete, these two materials were chosen for a comparison of the individual effects. Also for a more accurate comparison concrete and mortar specimens were made of different mixtures where the composition can be seen in the Tab. 5.1. The mortar mixtures were identical to the concrete mixtures, but without aggregates larger than 4 mm. It is known from [74] that various admixtures and additives affect the microstructure and porosity. The purpose of this work is to investigate how different mixtures react to an electric current. The samples were placed in 1% lime water after preparation and all further procedure is shown in the Fig. 5.3.

Component	cA	cB	cC	mA	mB	mC
CEM I 42.5R	230.5	-	207.4	230.5	-	207.4
CEM II/A-M(LL) 42.5R	-	230.5	-	-	230.5	-
Microsilica	-	-	23.0	-	-	23.0
Water	185.0	185.0	185.0	185.0	185.0	185.0
Sand 0-4 mm	1012.3	1012.3	1012.3	1289.0	1289.0	1289.0
Aggregate 4-8 mm	256.1	256.1	256.1	-	-	-
Aggregate 8-16 mm	512.1	512.1	512.1	-	-	-
Water/binder (w/b)	0.8	0.8	0.8	0.8	0.8	0.8

Table 5.1: Concrete and mortar samples composition in kg/m^3.

5.1.1 Preparation for chloride profile determination

Since the chloride profile on the samples was determined by leaching a small amount of sample powder of the individual layers, it was necessary to obtain the layers from the sample. The first three layers were grinded off two millimetres at a time using a diamond grinder, so a total of six millimetres were grinded off. For the samples that were subjected to the ponding test, the edges were cleaned of the acrylic coating beforehand, see Fig. 5.1.

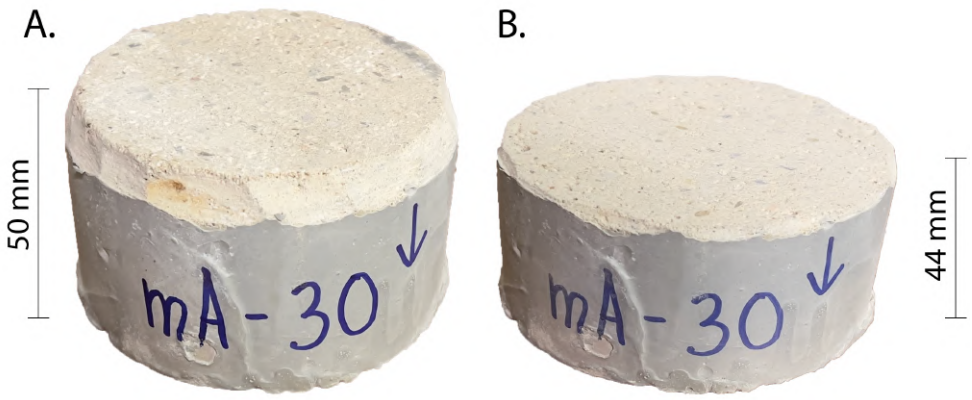

Figure 5.1: Sample before grinding (A.) and after grinding (B.) the first three layers.

Further layers were drilled in 5 mm layers through the whole sample for time reasons, as this is faster than grinding, see Fig. 5.2. For each sample, 12 holes were drilled approximately 10 mm apart to obtain sufficient sample to determine the chloride concentration.

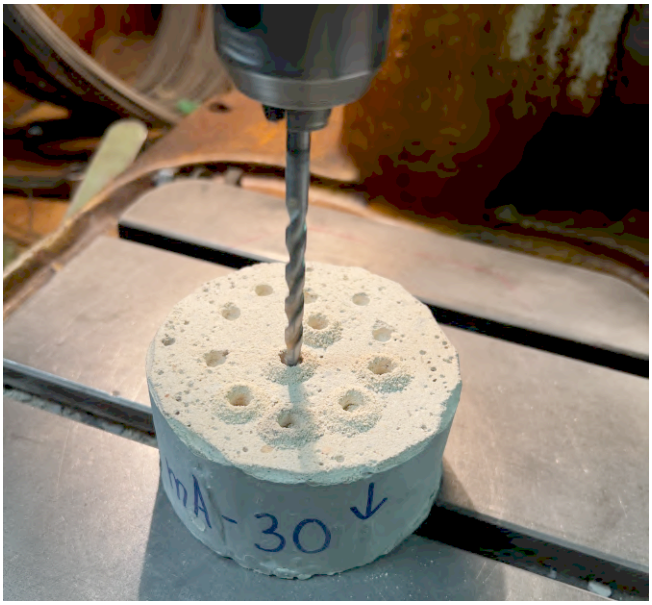

Figure 5.2: Drilling of the fourth layer of five millimeters.

5.2 Experimental plan

1. The first set of the samples was removed from the lime water after 90 days and placed in 3% NaCl solution. The samples were removed from the water after 30, 60 and 120 days and placed successively in the oven at 50 °C. On the first half of the sample set the chloride profile was determined and on the second half of the sample set chloride extraction was performed, see Fig. 5.3, set 1. Determination of chloride profile and MIP could not be done for time reasons.

2. The second set of samples was after 120 days removed from 1% lime water and a Direct Current (DC) test was immediately performed on the fully saturated samples, see Sec. 5.3.2. After the test, the samples were placed in an oven for 2 days at 50 °C. After two days, the samples were vacuum saturated with potable water and stored for 30 days in 3% NaCl solution. The samples were then placed in an oven for 2 days at 50 °C. A chloride profile was for concrete samples determined, see Fig. 5.3, set 2..

3. The third set of samples was used to study effect of electric current on the concrete microstructure, especially to study changes in porosity. After 120 days the samples were removed from 1% lime water, and Open Porosity (OP) was measured, see Sec. 5.3.2. One round of OP took approximately 20 days of drying in the oven at 50 °C where one of the samples from cA set were after test taken to SEM, TGA and XRD analysis. Right after that the rest of the samples were saturated and **DC test was performed**, see Sec. 5.3.2. Immediately after DC test the second OP measurement was made to determine the effect of the flow of electric current on the porosity. One of the samples from the cA set was after test taken to SEM, TGA and XRD analysis again to determine difference of the microstructure and chemical composition before and after DC test. Right after the second OP was the rest of the samples saturated and penetrated with chlorides by electric current (see Fig. 5.3, set 3.), and then MIP was performed on concrete samples. SEM, TGA and XRD analysis was only performed on the cA test due to capacity and time reasons.

4. The fourth set of samples was after $\sim$560 days laying in 1% lime water removed and injected by nanosilica. Then on the first half of samples from each set ponding test was performed and on the second half of the set an Accelerate Chloride Penetration Test (ACPT) was performed, see Sec. 5.3.2. After ponding test, the chloride profile was determined, see Fig. 5.3, set 4. Due to capacity and time reasons it was determined only on concrete samples.

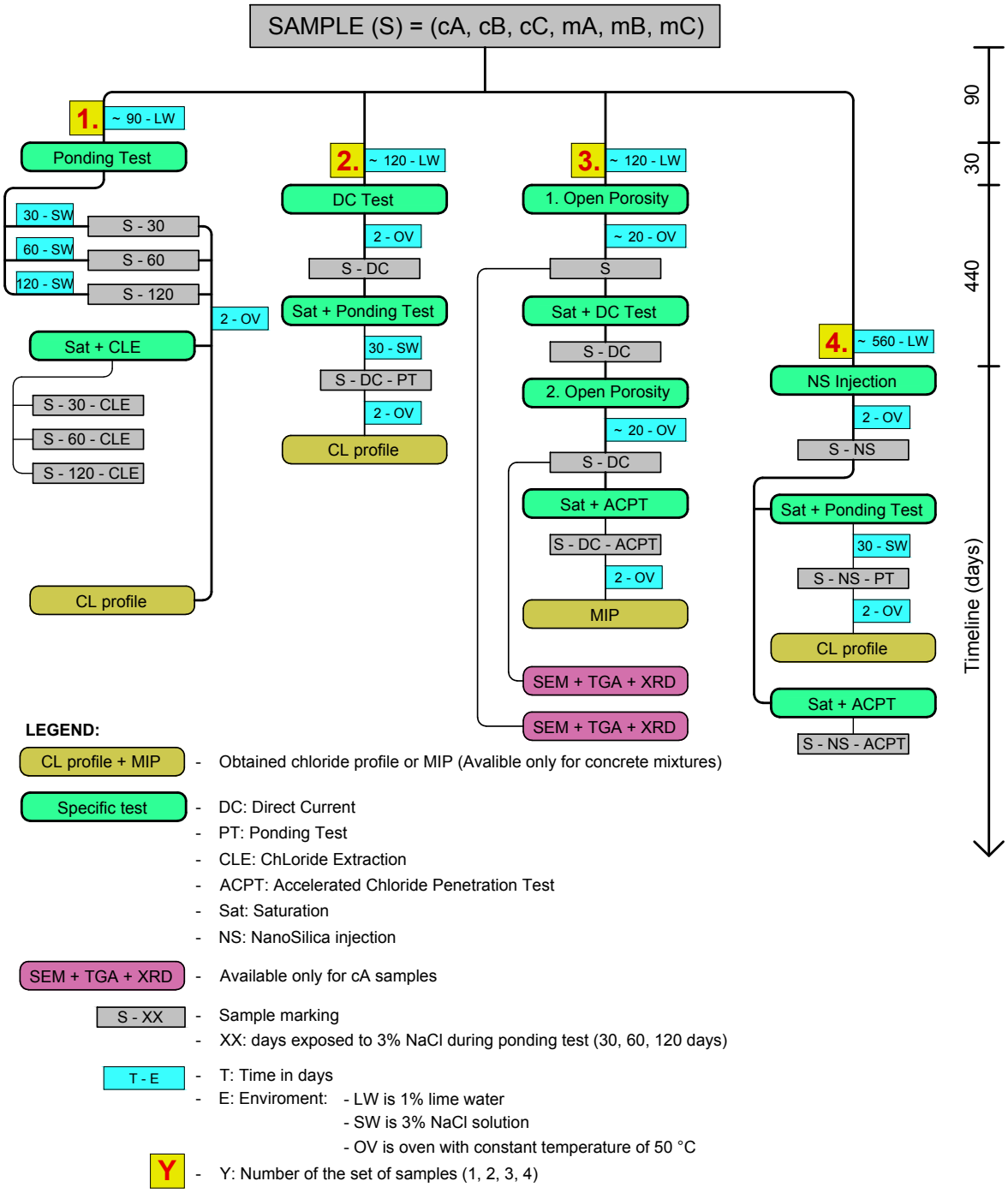

Figure 5.3: Flow chart.

5.3 Experimental tests, results and discussion

5.3.1 Open porosity

Open porosity (OP) was measured from fully saturated samples which were placed in an oven at 50 °C, and the sample's mass was then sequentially measured to detect the water loss. Samples were considered dried if the daily water loss ratio to the fully saturated sample was less than 0.1% for at least 2 consecutive days. The period for which the samples have usually dried is approximately 20 days, see Fig. 5.3. The statistics were performed on the basis of two samples from each mixture. The main purpose of measuring the open porosity before and after the DC test is to determine the effect of the passage of electric current on the open porosity of concrete and mortar.

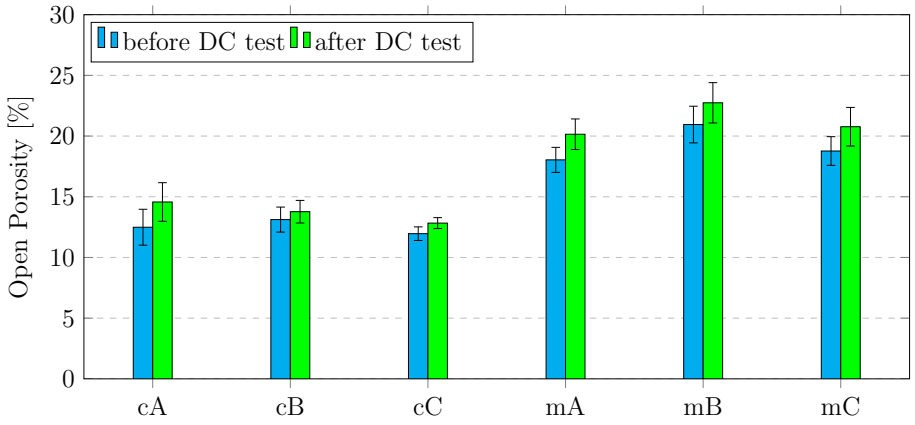

Figure 5.4: Open porosity of samples before loaded by electric current and after.

Label	cA	cB	cC	mA	mB	mC
	ϕ_{OP}[%]	ϕ_{OP}[%]	ϕ_{OP}[%]	ϕ_{OP}[%]	ϕ_{OP}[%]	ϕ_{OP}[%]
before DC	12.5 ± 1.5	13.1 ± 1.0	12.0 ± 0.6	18.0 ± 1.0	20.9 ± 1.5	18.8 ± 1.2
after DC	14.6 ± 1.6	13.8 ± 0.9	12.8 ± 0.4	20.1 ± 1.3	22.7 ± 1.7	20.8 ± 1.6
increase [%]	16.8	5.3	6.7	11.7	8.6	10.6

Table 5.2: Open porosity of virgin samples and samples subjected to DC test.

The results of open porosity indicate a different influence of the electric current on the different concrete and mortar mixtures. In the Fig. 5.4 it is possible to observe the increase in porosity for all six mixtures. However, the greatest increase in porosity is shown by the mixture of cA and mA, where an increase in porosity by 16.8% was observed in both cases. The highest resistance to the passage of electric current, i.e. the lowest change in porosity, was exhibited by the cB mixture, where porosity increased by only 5.3%, and by the mB mixture, where porosity increased by 8.6%, see Tab. 5.2.

5.3.2 Accelerated tests

Direct Current (DC) Test setup

The DC test which was used in this thesis was inspired by the above mentioned RCPT. During the DC test, the voltage was set only to 20 V with the duration of 24 hours to better simulate settings used for chloride extraction on real structures. Also, the NaOH with 0.3 M concentration was present in both chambers. No chlorides were present in the DC test. The scheme of the experiment is shown in Fig. 5.5. The stainless steel electrodes were placed in two chambers filled with 0.3 M NaOH solution. The concrete sample was placed between both chambers to create the conductive path. The electric current is conducted through continuously connected pores filled with pore solution. During the DC test the voltage was set constant and the current was measured. The total passed charge, Q, can then be expressed by formula

$$Q = \int I(t)dt, \tag{5.1}$$

where I is the the current, and t is the time.

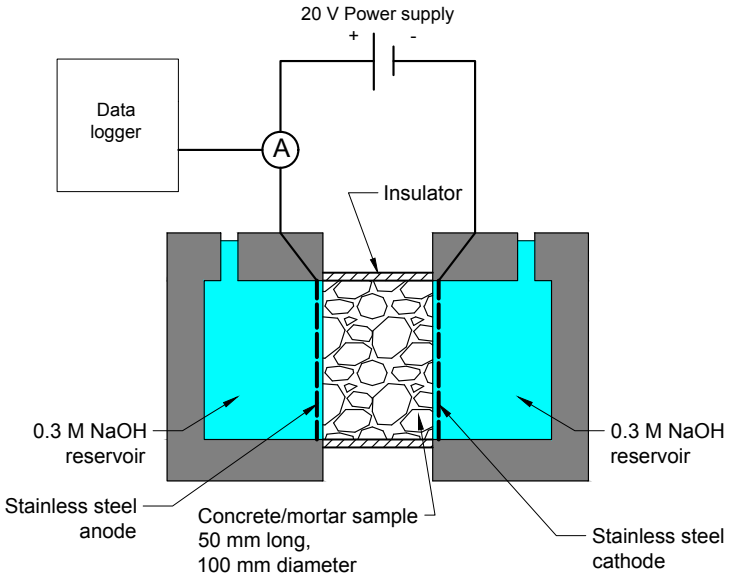

Figure 5.5: Scheme of the DC test.

Direct Current (DC) Test results

Concrete samples cA, cB and cC show the expected trend of relatively constant electric current, where sample cA shows a higher electric current waveform compared to samples cB and cC, see Fig. 5.6. The electric current waveform for the mortar samples mA and mB is higher than that for the mC samples. However, the trend is the same for all mortar samples. The electric current increases at the beginning of the test, followed by a more constant current waveform. For both the mortar and concrete samples, the

largest amount of electric current passed through the cA and mA mixtures. Typical curves are shown in Fig. 5.6.

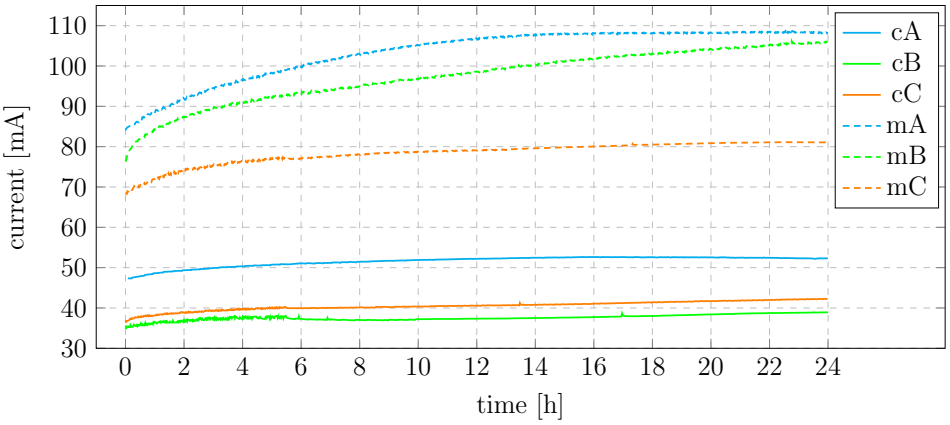

Figure 5.6: Change of the electric current over time during DC test.

By integrating the electric current in the time, the electric charge C for the individual samples was obtained and the results can be seen in Fig. 5.8 and in Tab. 5.3.

Accelerated Chloride Penetration Test (ACTP) setup

The ACPT test used in this thesis was identical to the DC test with only one difference. The chamber to which the negative electrode was connected was filled with 3% NaCl solution instead the NaOH with 0.3 M concentration, see Fig. 5.7.

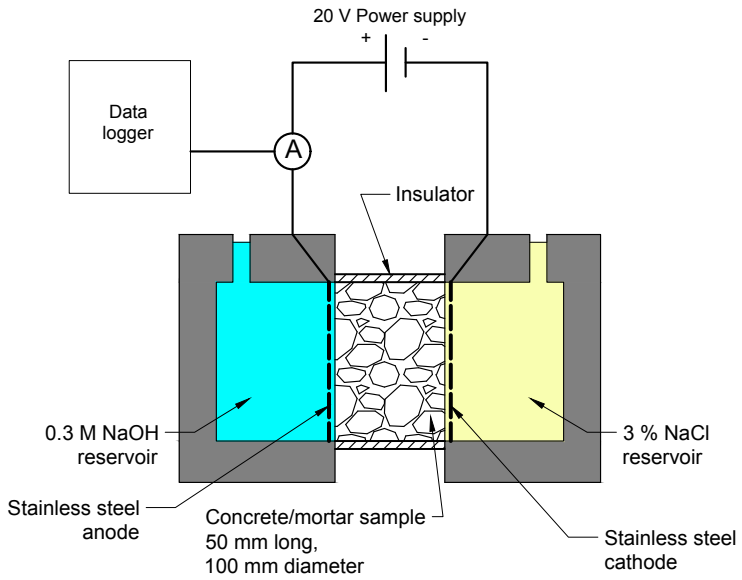

Figure 5.7: Scheme of the ACPT test.

Direct Current Test vs Accelerated Chloride Penetration Test results

Similarly to the results from the DC test, the ACPT also recorded a significantly higher passage of electric current through the mortar specimens than through the concrete specimens. The highest passage of electric current for both mortar and concrete specimens was recorded for the cA mixture. The smallest passage was recorded for concrete samples through the cB mix and for mortar samples through the mC mix.

The results were processed into a graph, see Fig. 5.8. Despite the fact that the mobility of OH^- ions is approximately 2.5 times higher [98, 99], ACPT tests with NaCl solution showed a higher electric current throughput. Also, the samples subjected to ACPT tests were approximately 20 days older, so their microstructure should be more mature. The reason why in all cases there is an increased electrical current throughput in the samples subjected to ACPT is most likely that all samples subjected to ACPT were previously subjected to the DC test (see Fig. 5.3, set 3.), which opened up the porosity (see Fig. 5.4) and allowed the ions to pass through more easily.

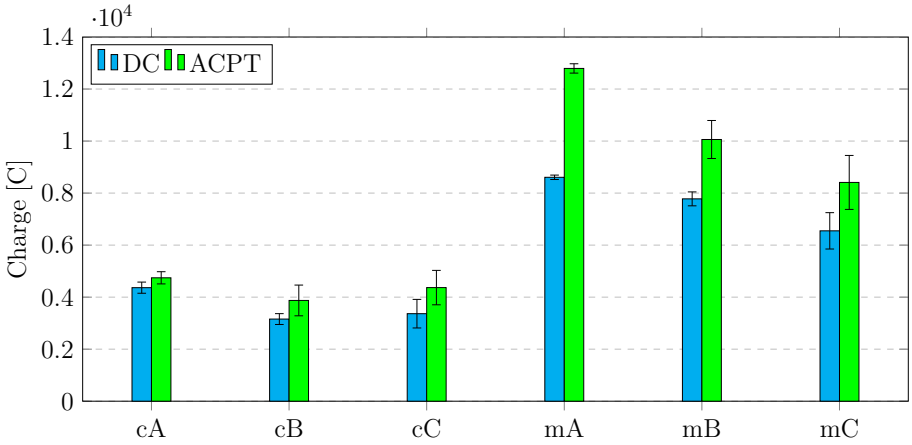

Figure 5.8: Total charge measured during DC test and ACPT.

The largest change in the electric current passage (see Tab. 5.3) was observed for the mortar samples mA, specifically by 48.6%. This is in consistent with the results in Fig. 5.4, where the largest change in porosity was recorded for the cA mixture. However, the largest change in porosity after passing through the electric current was recorded for the cA mixture, where only one electrical test was performed. In this case, the electrical test was performed twice on the individual samples, first the DC test and then the ACPT. From this it can be concluded that the repeated electrical test does not have as much effect on the concrete mixture cA as it has on the mixture cC, see Tab. 5.3.

The above-mentioned statements about the effect of repeated electrical testing do not describe the behavior of the mortar samples. The mA mortar mixture shows significantly the largest change in the electric current passage, specifically by 48.6%. The

Label	cA Q[C]	cB Q[C]	cC Q[C]
DC	4364 ± 215	3157 ± 208	3364 ± 549
ACPT	4743 ± 235	3873 ± 591	4367 ± 661
relative change [%]	8.7	22.7	29.8
Label	mA Q[C]	mB Q[C]	mC Q[C]
DC	8607 ± 85	7778 ± 268	6549 ± 699
ACPT	12792 ± 180	10061 ± 731	8410 ± 1037
relative change [%]	48.6	29.4	28.4

Table 5.3: Total charge passed during DC test and ACPT.

mixture cB shows increase of electric current passage by 29.4% and the mC mixture shows the smallest change, specifically by 28.4%, see Tab. 5.3. In the case of mortar mixtures, the mA mixture appears to be the most prone to multiple electrical loads. Since the highest charge has passed through it, it means that its resistance is lowest.

Chloride Extraction (CLE) Test setup

The CLE test used in this thesis had an identical setup as the ACPT test with the change of polarity. For the CLE test it was important to place the side through which the chlorides were penetrated into the sample at the positive electrode, see Fig. 5.9, yellow side. Chloride ions travel to positive electrode and are extracted from the sample.

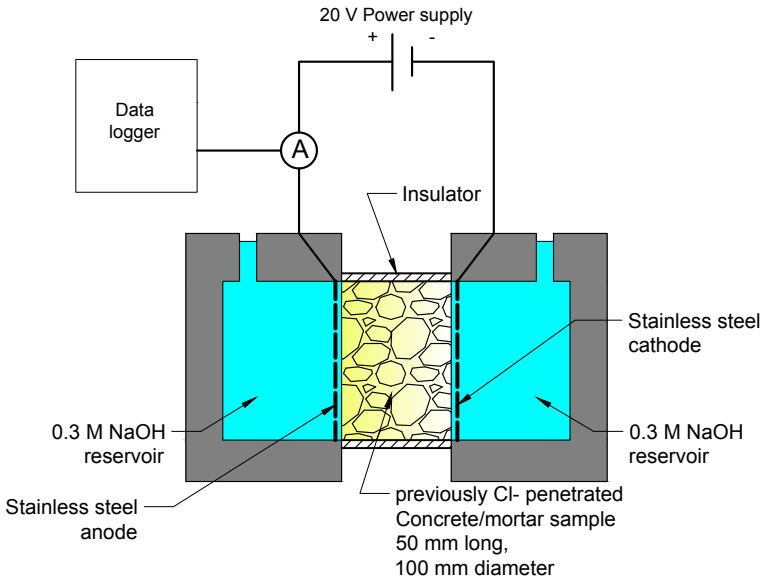

Figure 5.9: Scheme of the CLE test.

Chloride Extraction (CLE) Test results

The results show that through concrete and also through mortar mixtures cA and mA the most electric current passed compared to the other samples, which is the same trend as was recorded with the change of porosity (see Fig. 5.4). It also does not contradict the hypothesis with the results where two electrical tests were performed on the samples (see Fig. 5.8), since the CLE test was performed on samples that were not previously subjected to the electrical test, see Fig. 5.3, set. 1.

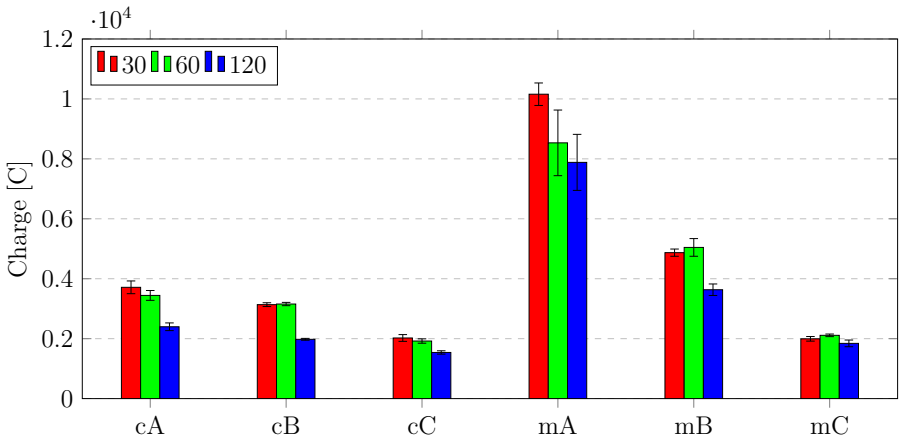

Figure 5.10: Total charge passed during CLE tests for samples exposed to ponding test for 30, 60 and 120 days.

Label	cA Q[C]	cB Q[C]	cC Q[C]
30	3714 ± 213	3135 ± 63	2023 ± 113
60	3443 ± 164	3156 ± 55	1921 ± 73
120	2398 ± 128	1978 ± 31	1540 ± 56
Label	mA Q[C]	mB Q[C]	mC Q[C]
30	10157 ± 375	4870 ± 121	1995 ± 77
60	8534 ± 1095	5045 ± 295	2112 ± 43
120	7883 ± 935	3633 ± 192	1843 ± 112

Table 5.4: Total charge passed during CET tests.

The mortar mixtures at 60 days, except in the case of mA, almost copy the behaviour of those at 30 days. This could mean that no major change in the microstructure has taken place in 30 days. However, at 120 days there is an evident decrease in the electrical current passage in all mixtures, resulting in a mature microstructure that was present at the time of hydration, see Fig. 5.10.

Nanosilica (NS) Injection Test setup

The setup of the NS injection can be seen in Fig. 5.11. In the chamber in which the stainless steel net was attached to the minus pole was a nanosilica solution with the following properties: density = 1.4 g/cm^3, solid particle content = 50 %, H_2O = 50 %, particle size = 20 - 250 nm and pH = 9.5. The commercial name of the used nanosilica colloidal sodium stabilized solution is Akzo Nobel Levasil CB8. The principle is that NS travelling from the negative pole to the positive pole and fill the porous system.

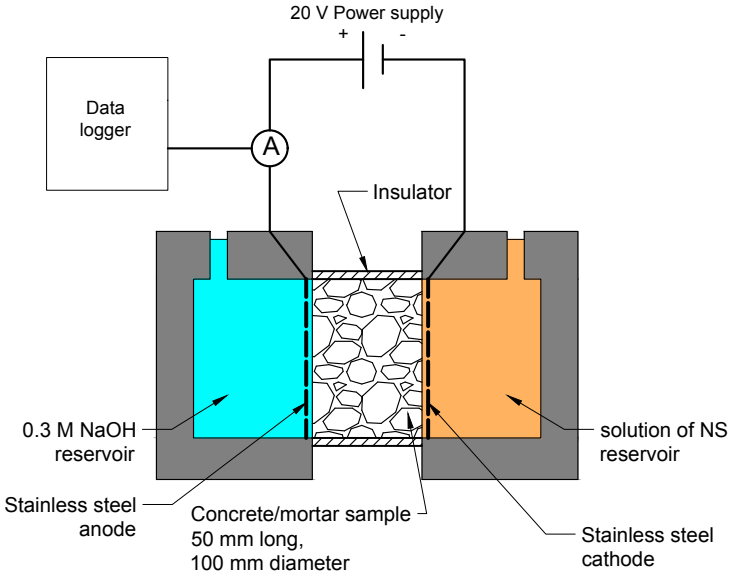

Figure 5.11: Scheme of the NS injection test.

Nanosilica Injection vs Accelerated Chloride Penetration Test results

Similarly to the results from the DC test, ACPT, or CLE test, the NS injection test

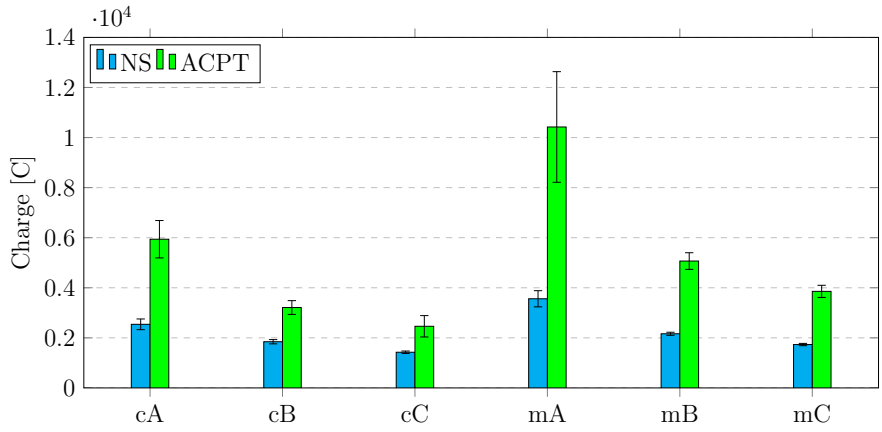

Figure 5.12: Difference of charge passed during NS injection and ACPT.

recorded the highest electric current passage through the concrete mixtures cA and the mortar mixtures mA and the lowest passage through the mixtures cC and mC, see

Fig. 5.12. However, in the NS injection test, the difference in electric current passage between the concrete and mortar mixtures was not as significant as in the previous tests. The passage of electric current was by 38% less for the cB mixture and by 78% less for the cC mixture compared to the cA mixture. For the mortar samples, compared to the mA mixture, a decrease by 65% for the mB mixture and a decrease by up to 105% for the mC mixture was recorded, see Fig. 5.5.

Label	cA	cB	cC
	Q[C]	Q[C]	Q[C]
NS	2541 ± 214	1845 ± 85	1426 ± 48
ACPT	5939 ± 747	3211 ± 275	2462 ± 427
relative change [%]	133.7	74.0	72.7
Label	mA	mB	mC
	Q[C]	Q[C]	Q[C]
NS	3561 ± 323	2163 ± 61	1733 ± 46
ACPT	10422 ± 2210	5068 ± 332	3857 ± 243
relative change [%]	192.7	134.3	122.6

Table 5.5: Total charge passed during NS injection and ACPT.

The passage of electric current during injection with the nanosilica was the highest for the cA and mA mixtures, which corresponds to the highest increase in porosity for these mixtures, see Fig. 5.4. The highest resistance to electric current was produced by the cC and mC mixtures.

The differences between the electrical passages during ACPT and NS injection tests were as follows. The largest differences in the passage were noted for the cA and mA samples, where an increase in the electrical current passage by 133.7% was recorded for the cA blend and an increase in the passage of the electric current by 192.7% for the mA blend. The smallest differences in passage between the individual tests were recorded for the cC mixture, where an increase by 72.7% was recorded, and for the mC mixture, where an increase by 122.6% was recorded.

The graph in Fig. 5.12 shows that for all mixtures, the current passage during nanosilica injection is much less than the passage during ACPT what is the expected trend. This could be due to the fact that nanosilica particles are larger than chloride ions and it is more difficult for them to pass through the concrete and mortar pore system. It could also be due to the fact that the nanosilica particles begin to aggregate together and form even larger clumps which are even more difficult to pass through the porous system. Another big reason is the decrease in the amount of charge that NS carries. In suspension, the electrical charge of NS particles influences their colloidal

stability. A decrease in the charge lead to particle aggregation. This was noticed after the NS injection test, which may have led to an overall lower electric current passage.

Figure 5.13: Aggregation of nanoparticles after NS injection test.

Accelerated Chloride Penetration Test before Nanosilica Injection Test vs after Nanosilica Injection Test

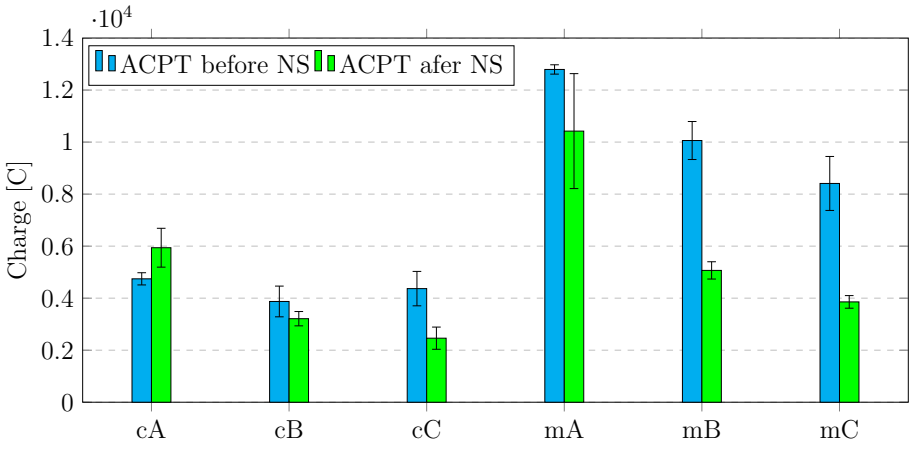

Figure 5.14: Difference of charge passage during ACPT before NS injection and after.

Label	cA Q[C]	cB Q[C]	cC Q[C]
ACPT before NS	4743 ± 235	3873 ± 591	4367 ± 661
ACPT after NS	5939 ± 747	3211 ± 275	2462 ± 427
relative change [%]	25.2	-17.1	-43.6
Label	mA Q[C]	mB Q[C]	mC Q[C]
ACPT before NS	12792 ± 180	10061 ± 731	8410 ± 1037
ACPT after NS	10422 ± 2210	5068 ± 332	3857 ± 243
relative change [%]	-18.5	-49.6	-54.1

Table 5.6: Total charge measured during ACPT before and after NS injection.

In Fig. 5.14 is a graph showing the reduction of the electric current passage during ACPT in almost all samples that were previously treated with nanosilica injection. This could mean that the nanosilica fills the porous system. The largest decrease in electric current passage was observed for the concrete sample cC and for the mortar samples mB and mC. This could mean that the nanosilica injection has greatest effect for these mixtures. Interestingly, for the concrete sample cA a decrease in the electric current passage was not recorded, but on the contrary an increase by 25.2% was recorded, see Tab. 5.6.

5.3.3 Ponding (diffusion) test

Before the ponding test, the samples were removed from the lime water and dried naturally for one day in a room at a temperature of approximately 20 °C and a humidity of approximately 50%. The surface drying was only done in order to be able to properly apply the acrylic layer, because samples subjected to the ponding test were coated with a water-impermeable acrylic sealant. One base and the lateral area of the cylinder, which is the shape of each sample, were painted, see Fig. 5.15.

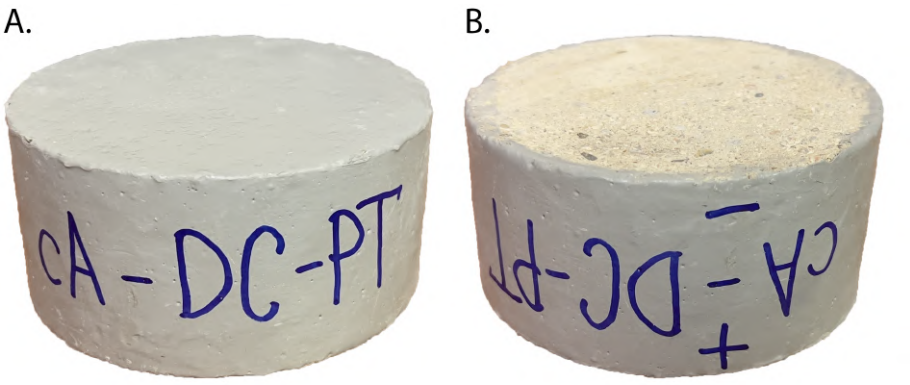

Figure 5.15: Coating one of the samples subjected to ponding test. View of the sample from above (A.) and below (B.).

The samples were left in the room after application of the acrylic primer. After 4 hours, another layer of acrylic primer was applied and the samples were left in the room for another day to allow the primer to dry thoroughly. The samples were then placed in tap water for approximately one day to ensure that the samples were fully saturated before being placed in the solution. The samples were then placed in 3% NaCl solution (see Fig. 5.16) for 30, 60 and 120 days, see Fig. 5.3 for more information.

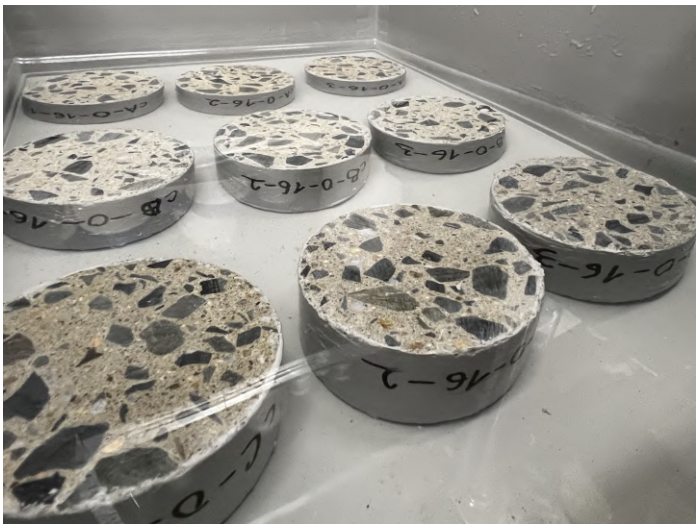

Figure 5.16: Samples fully submerged in 3% NaCl solution.

By fitting an error function (see Eq. 4.10), the surface chloride concentration C_s and effective diffusion coefficient D_{eff} were obtained. The fitting was performed using the method of the least squares, where the smallest deviation of the curve from the measured points is searched. To obtain the parameters, python code was created, which can be seen in appendix Chapter 8. On the basis of these parameters, the concentration at individual depths was predicted.

The calculation of the amount of chloride absorbed in the sample can be calculated from chloride concentration profile, $C(x)$. The amount of chlorides in the sample w_{Cl} [g] was estimated from fitted concentration profiles (see Eq. 4.10) as is graphically shown in Fig. 5.17.

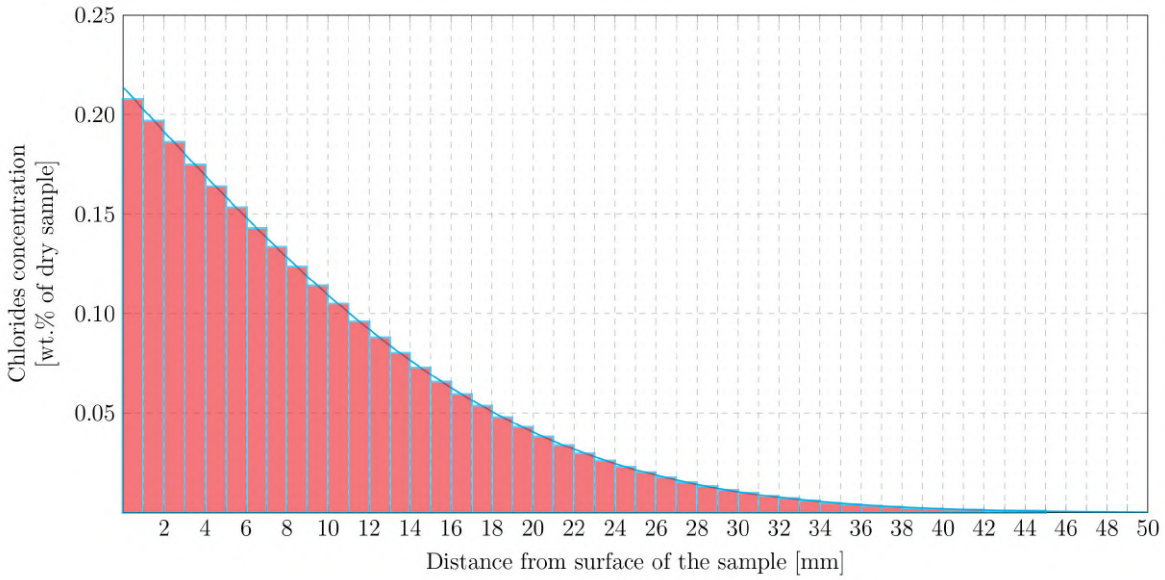

Figure 5.17: Integration scheme used for calculation of the total amount of chlorides entering the sample.

To estimate the area under the graph described by the Eq. 4.10, a numerical integration method, also known as trapezoidal rule was used. Then, the formula for the w_{Cl} calculation is:

$$w_{\mathrm{Cl}} \approx \rho_{\mathrm{M}}.V_{\Delta x}.\frac{\Delta x}{2}.\sum \left(C_{[\mathrm{i}]} + C_{[\mathrm{i+1}]}\right), \tag{5.2}$$

where Δx is the integration step, which is 1 mm, ρ_{M} is a bulk density of the mixture and $\mathrm{V}_{\Delta x}$ is a volume of 1 mm section of the sample. The summation runs from i = 0 to i = n-1, with n being the number of data points, which is 50 in this case.

Ponding test results of the samples from the set 1.

The samples from the set 1. were subjected to the ponding test immediately and no other test preceded it, see Fig. 5.3.

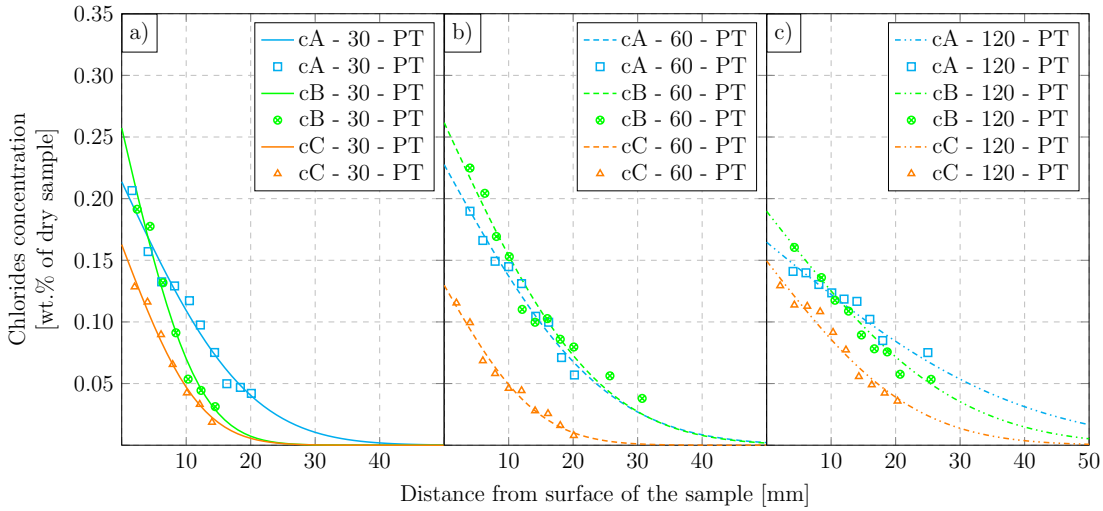

Figure 5.18: Comparison of chloride concentrations at a given depth for different mixtures. Samples were subjected to ponding test for a) 30, b) 60 and c) 120 days. Individual marks represent measured data from which the curves were fitted.

Fig. 5.18 shows concentration of individual mixtures at the same time. In all cases, the cC mixture has a lower surface and depth chloride concentration compared to the other samples. Also, in all cases the surface chloride concentration is highest for the cB mixture, but decreases more rapidly with depth penetration than the chloride concentration in the cA samples. Overall, the cC mixture shows the highest resistance to chloride penetration for all times of ponding test.

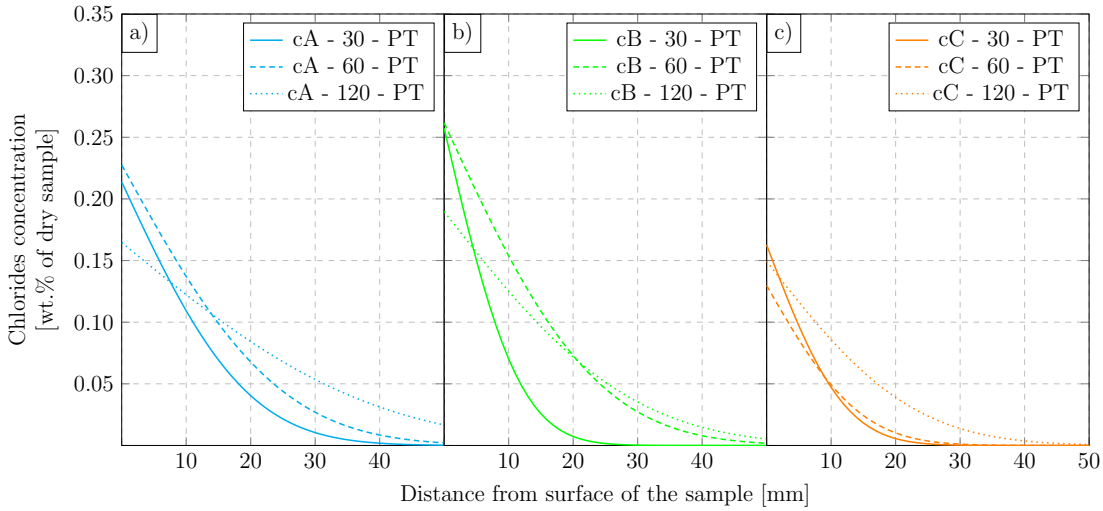

Figure 5.19: Comparison of chloride concentrations for mixture a) cA, b) cB, c) cC for different times of chloride exposition.

In Fig. 5.19 it is possible to observe individual mixtures in various exposure times. In every single graph, the depth concentration for a chloride exposure time of 30 days is the lowest, which is the expected trend. Also, for a time of 120 days, the depth concentration of chloride is greatest for all samples. For samples cA and cB at 120 days, the surface chloride concentration is lower than at 30 and 60 days. This may be due to fitting, as the higher concentration at greater depth flattens the overall curve more and thus lowers the surface concentration.

Days		30			60			120	
Samples	cA	cB	cC	cA	cB	cC	cA	cB	cC
C_s [wt.%]	0.214	0.257	0.163	0.228	0.262	0.130	0.165	0.190	0.150
C_s change [%]	ref	20	-24	ref	15	-43	ref	15	-9
D_{eff} [.10^{-11} m^2/s]	4.47	1.60	1.72	3.56	3.29	1.25	4.48	2.48	1.53
D_{eff} change [%]	ref	-64	-62	ref	-8	-65	ref	-45	-66
w_{Cl} [g]	44.98	32.35	21.28	60.03	66.43	20.41	65.57	58.65	36.68
w_{Cl} change [%]	ref	-28	-53	ref	11	-66	ref	-11	-44

Table 5.7: Diffusion parameters obtained from fitting of measured data.

The individual results can also be seen in the Tab. 5.7 where the exact values from which the graphs were made using the Eq. 4.10 are shown. In the mentioned Tab. 5.7 it can be seen that the diffusion coefficient for the samples cA is the largest for all times and for the samples cC is the smallest for all times, except for the time of 30 days.

The amount of chloride is highest for 30 days and 120 days for the cA mixture and lowest for the cC mixture at all times. For example, at the 30-day ponding test time, the relative change in amount of chlorides is -28% for the cB mixture and -53% for the cC mixture compared to the cA mixture. In all cases, the chloride amount is lowest for the cC mixture. In the case of a ponding test lasting 60 days, it is 66% lower compared to the cA mixture. Also, for cA and cC mixtures, the highest chloride amount was recorded for mixtures subjected to the ponding test for 120 days, which is an expected trend.

There was also recorded a decrease in the diffusion coefficient of the mixtures cB and cC compared to the mixture cA. This indicates that the cA mixture provides easier diffusion to chlorides. The individual results also confirm the trend obtained from the chloride amount. In Fig. 5.20 it can be observed that the values of the effective diffusion coefficient are similar for different times and each mixture. However, different mixtures have different effective diffusion coefficients which is related to chloride binding, and different microstructure and porosity of the mixtures.

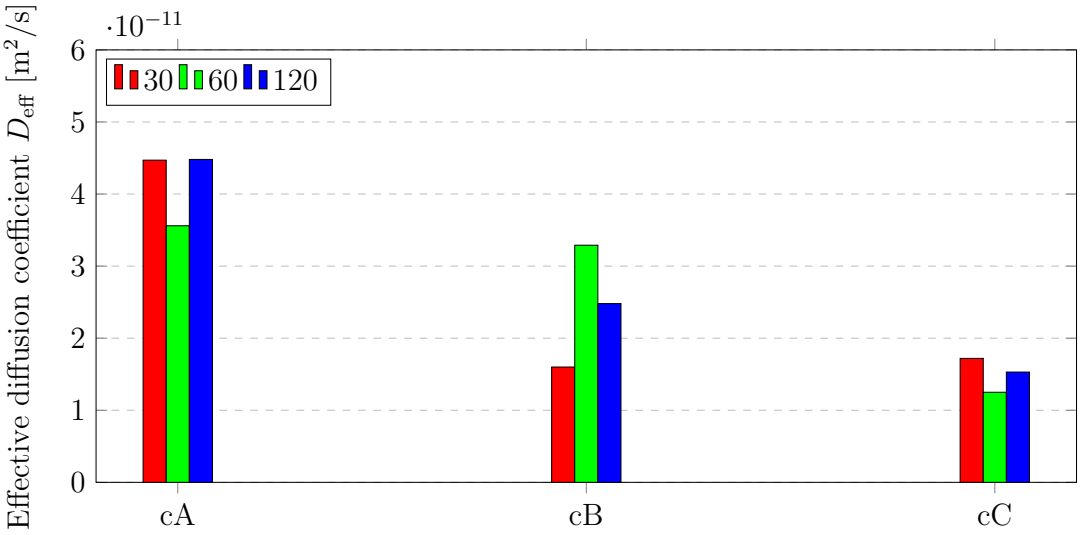

Figure 5.20: Comparison of effective diffusion coefficient D_{eff} for individual concrete mixtures.

Ponding test results of the samples from the set 2.

The samples from the set 2. were subjected to the ponding test right after the preceding DC test, see Fig. 5.3. This is the difference between set 1. and set 2., which allows to attribute the change in the results of the individual sets to the DC test.

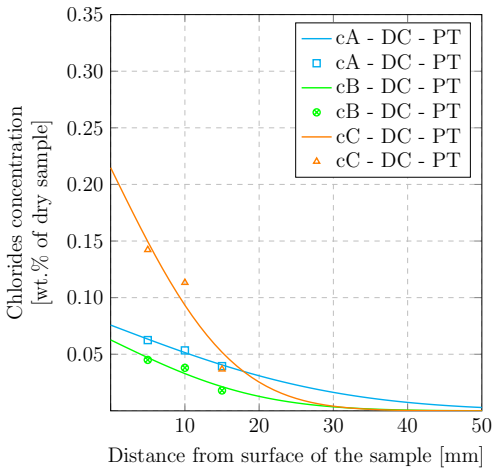

Figure 5.21: Comparison of chloride concentrations at a given depth for different mixtures after DC test. Individual marks represent measured data from which the curves were fitted.

Fig. 5.21 shows graph comparing individual mixtures. It is possible to observe a significantly reduced surface chloride concentration in samples cA and cB. This may be due to the change in microstructure after the DC test. From this it is possible to conclude that sample cC is not as prone to electric current as samples cA and cB. It is also possible to observe an increased concentration of chloride in the depth of sample

cA, which was also confirmed in the samples from the set 1., see Fig. 5.18.
The individual results can also be seen in the Tab. 5.8, where is possible to see that the diffusion coefficient for the samples cA is the largest and diffusion coefficient for the samples cC is the smallest which is in correlation with results from set 1., see Tab. 5.7.

Samples	cA	cB	cC
C_s [wt.%]	0.076	0.063	0.215
C_s change [%]	ref	-17	183
D_{eff} [.10^{-11} m^2/s]	11.30	4.78	3.16
D_{eff} change [%]	ref	-58	-72
w_{Cl} [g]	24.91	13.67	37.89
w_{Cl} change [%]	ref	-45	52

Table 5.8: Diffusion parameters for samples subjected ponding test after DC test.

For the value of the effective diffusion coefficient D_{eff}, a decrease compared to the cA mixture by 58% for the cB mixture and by 72% for the cC mixture was recorded. This confirms the trends obtained from tests where natural diffusion has been performed. However, the total amount of chloride was higher in the cC mixture than in the cA mixture, which may indicate that the passage of the electric current affects this mixture the most.

Ponding test results of the samples from the set 4.

From Fig. 5.3, is possible to see that the samples from the set 4. were subjected to the ponding test after the preceding nanosilica injection test. This allows us to compare the differences between samples that have been injected with nanosilica with samples through which an electric current has passed and with samples that have only been subjected to a ponding test.

In the Fig. 5.22 it can be seen again that the depth concentration of chloride after the ponding test performed on the samples injected with nanosilica is the highest for the cA sample and the lowest for the cC sample. The surface concentration is highest for sample cC. However, the values of surface concentrations are not very different between the samples.

In the Tab. 5.9 it is possible to see that the highest values of the effective diffusion coefficient were exhibited by the sample cA and the lowest by the sample cC. The effective diffusion coefficient of the cB mixture was 40% lower compared to the cA. It was also lower for the cC mixture by 63%. The change in w_{Cl} was lower compared to the cA mixture by 27% for the cB mixture and by 28% for the cC mixture, see Tab. 5.9. It is evident that the effective diffusion coefficient after NS injection has

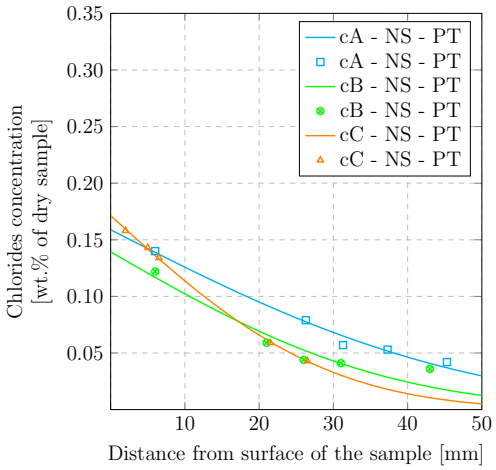

Figure 5.22: Comparison of chloride concentrations at a given depth for samples injected with nanosilica after ponding test. Individual marks represent measured data from which the curves were fitted.

increased significantly compared to that after DC test.

Samples	cA	cB	cC
C_s [wt.%]	0.159	0.139	0.171
C_s change [%]	ref	-13	8
D_{eff} [.10^{-11} m^2/s]	27.77	16.74	10.19
D_{eff} change [%]	ref	-40	-63
w_{Cl} [g]	74.04	53.98	53.63
w_{Cl} change [%]	ref	-27	-28

Table 5.9: Diffusion parameters for samples injected with nanosilica after ponding test.

Comparison of chloride profiles between individual sets

Samples were compared between sets with only 30 days of chloride exposure, since in the second and fourth sets the samples were subjected to the ponding test only for this length of time. Apart from the surface chloride concentration, a slight increase in the deep chloride concentration can be observed for all mixtures after the DC test. This may be due to the opening of the porosity after the passage of the electric current and the later allowing the chlorides to travel deeper. A similar situation is the case for samples injected with nanosilica. However, the expectation was that the injection of the nanosilica would fill the microstructure and prevent further chloride penetration. It turned out that the injection of the nanosilica had such an effect on the microstructure that in all cases the depth concentration of chloride increased significantly, see Fig. 5.23.

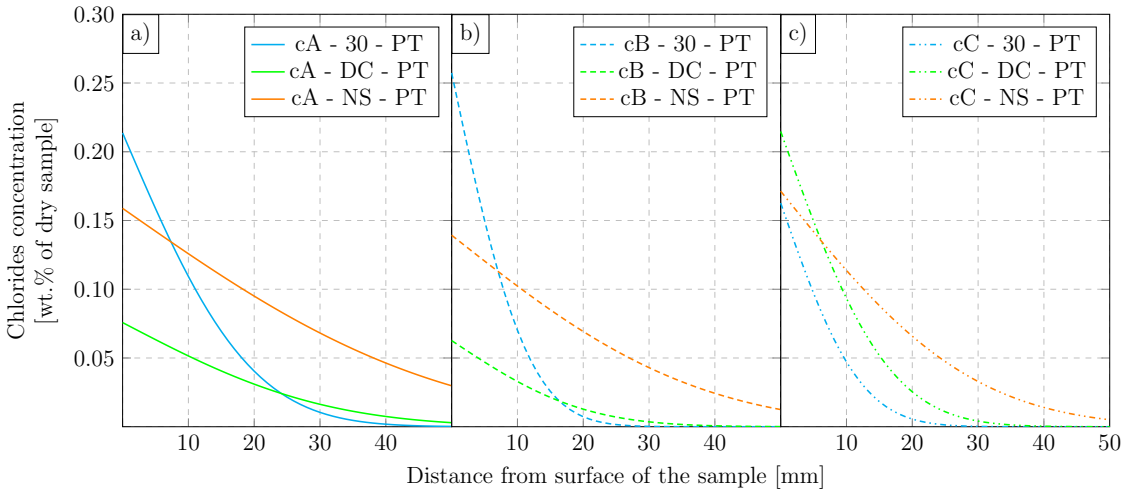

Figure 5.23: Comparison of chloride concentrations for mixture a) cA, b) cB, c) cC after different tests.

Samples	cA			cB			cC		
Tests	-	DC	NS	-	DC	NS	-	DC	NS
C_s [wt.%]	0.214	0.076	0.159	0.257	0.063	0.139	0.163	0.215	0.171
C_s change [%]	ref	-65	-26	ref	-76	-46	ref	38	5
D_{eff} [.10^{-11} m^2/s]	4.47	11.30	27.77	1.60	4.78	16.74	1.72	3.16	10.19
D_{eff} change [%]	ref	153	521	ref	199	946	ref	84	492
w_{Cl} [g]	44.98	24.91	74.04	32.35	13.67	53.98	21.28	37.89	53.63
w_{Cl} change [%]	ref	-45	65	ref	-58	67	ref	78	152

Table 5.10: Comparison of parameters obtained from fitting of measured data.

In Tab. 5.10, it is possible to observe the specific values of surface concentrations and diffusion coefficients for the individual samples from each set. In the case of mixtures cA and cB, which were subjected to the DC and NS tests, the surface concentration of chloride is significantly reduced. In the case of the effective diffusion coefficient, an increase was observed compared to all mixtures that were not subjected to the electrical test. The increase in the diffusion coefficient is probably due to the change in microstructure after the passage of an electric current, specifically due to increased porosity. The results of the chloride amount were not as expected, as there was a higher amount of chloride in all samples injected with the nanosilica. An increase by 65% was recorded for the cA mixture, 67% for the cB mixture and 152% for the cC mixture. A similar trend did not occur in the samples subjected to the DC test for the cA and cB mixture. This is due to the lower surface concentration, which significantly reduces the total amount of chloride. In this case it is probably a measurement error. Also, the resulting curve was fitted from only three points, see Fig. 5.21.

5.3.4 Mercury intrusion porosimetry

MIP was performed on sample's fragments weighing ∼1.5 g. The measurements were performed on an AutoPore IV 9500 instrument for pore sizes ranging from 0.0015 µm to 130 µm.

MIP results of the samples from the set 3.

The results of the MIP analysis for the concrete samples from the set 3. can be seen in Tab. 5.11. Unlike the open porosity, MIP did not show significant changes between the samples. The results for cA mixture show increase in porosity of approximately 0.93% which agree with results obtained from OP, see Tab. 5.2. However, for cB mixture was found a decrease in porosity of 1.78% and for cC samples was found a decrease in porosity of 0.32% after the DC test. This is most likely due to the fact that pores with detectable MIP dimensions have increased their porosity and moved outside the detection interval of the MIP technique (4 nm - 200 µm). This change was then detected by OP (> 1 µm) as displayed in Fig. 5.2, and SEM (> 100 nm), see Fig. 5.12.

Label	cA [%]	cB [%]	cC [%]
before DC	15.69	16.25	16.21
after DC	16.62	14.47	15.89
absolute change	0.93	-1.78	-0.32

Table 5.11: Results of porosity determined by MIP.

In Fig. 5.24 the pore size distribution curves measured by MIP for individual samples which were loaded or non-loaded by the current are shown. For all three mixtures it is possible to observe a shift of the main porosity peak into the smaller values after the DC, which is in agreement with the study of Susanto et al. [13], where a similar shift was observable for mortar samples. Fig. 5.25 shows the changes in pore distribution in different intervals.

For all mixtures, there is evident increase of pore volume with a radius smaller than 0.01 µm after the DC test. The increase is accompanied by the decrease of pores volume in the range (0.01-0.1) µm also for all mixtures. The pores of a radius higher than 0.1 µm and smaller than 1 µm show increase in porosity for cB and cC samples while cA sample remain almost unchanged. The pores with a radius higher than 1 µm show increase for all samples. The most significant increase in porosity is for the cA sample where the increase of pores in the interval 1 µm - 130 µm by ∼14% was measured. The change in the distribution of the volume of pores is obvious, as are the trends. This means that after passing through an electric current, the distribution of

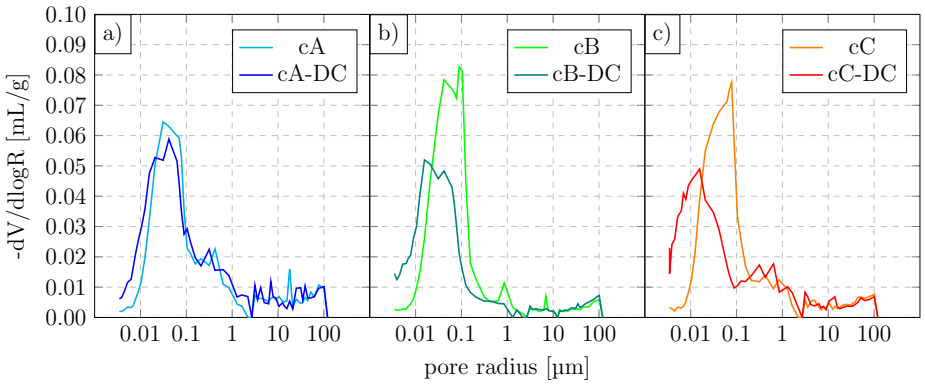

Figure 5.24: Pore size distribution curves of samples loaded and non-loaded by the electric current.

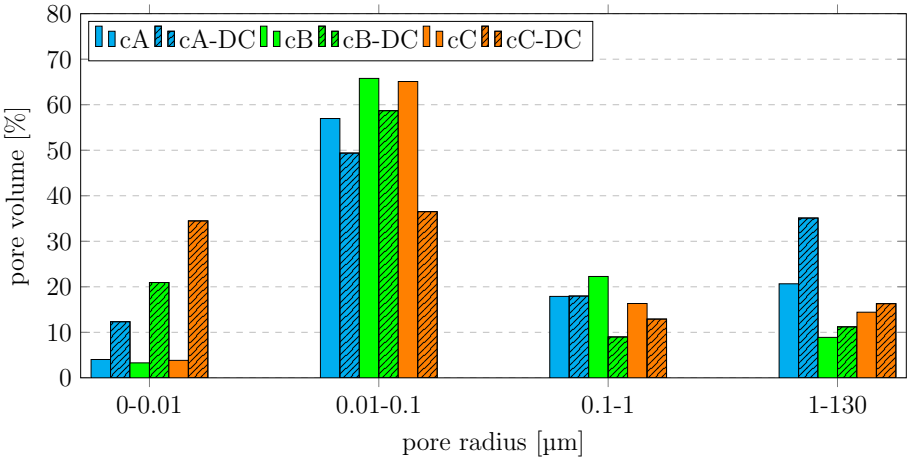

Figure 5.25: Pores volume changes in the different size ranges of samples loaded and non-loaded by the electric current.

the pores volume representation according to its radius changes, see Fig. 5.25.

5.3.5 Scanning electron microscopy and image analysis

The samples that were subjected to SEM and image analysis, i.e. the samples from the set 3. (see Fig. 5.3), were broken into smaller fragments. The pre-dried sample fragments were poured with epoxy resin into cylindrical moulds with a base diameter of 27 mm and a height of 60 mm, and then cut into 6 mm slices. For possible observation, the surface of the samples was treated, where the samples were polished with a Struers Tegramin 20 polisher. The polishing process was the same for all samples. The samples were polished with silicon carbide papers with grit sizes of 1200, 2000 and 4000. The samples were placed in a glass flask with technical alcohol and placed in an ultrasonic cleaner for two minutes between each polishing step. Prepared samples were observed by SEM Phenom XL. 10 BSE images were performed on each examined sample on the spots carefully chosen in the cement matrix. Thus, magnification was chosen from 1350× to 1600× to avoid aggregates.

In order to describe heterogeneous systems and their effective properties in a statistical sense, Representative Volume Element (RVE) have been introduced, where samples contain all phases in sufficient (statistically representative) quantities. For cement paste, this area is at least 100 × 100 μm^2. Totaly covering area for each set of samples in this work is 0.3 mm^2, which can be considered as sufficient for statistical analysis [106].

In addition to the correct sample preparation, the correct choice of threshold values for the individual phases. Thresholding was performed using MATLAB software based on the above mentioned Otsu's method. The threshold value of some images was manually adjusted due to the different contrast and brightness of the images.

Image analysis results

Image analysis was applied only to cA sample SEM-BSE images, see Fig. 5.3. Due to the aim of this work, only two phases were separated. The first phase was composed primarily of pores, but cracks and scratches were also present, as visible in Fig. 5.26. The second phase contains the rest of the phases, mainly hydration products, residual clinker, or small aggregates. It is also possible to see a different contrast in Fig. 5.26, specifically in Fig. 5.26 A, compared to Fig. 5.26 C. This is due to the presence of more phases, which are white in the SEM image, i.e. clinkers.

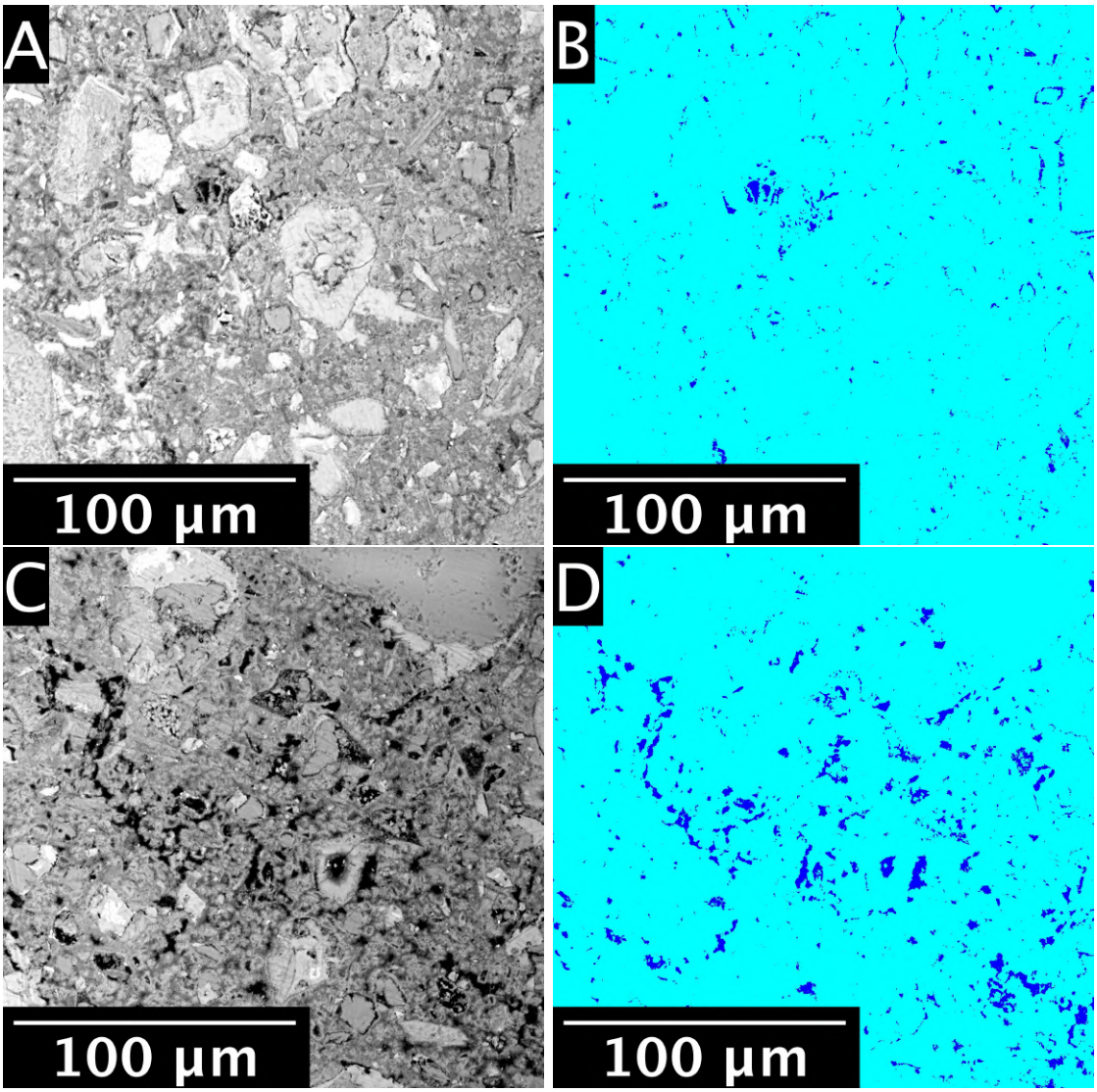

Figure 5.26: The typical SEM-BSE image of samples A) cA, C) cA-DC. Example of IA with phase separation: pores/cracks (blue), hydration products, residual clinker (cyan) of samples B) cA, D) cA-DC.

The results of image analysis and phase volume fraction are also shown in Tab. 5.12, where it is possible to observe an increase in porosity by 1.78% in concrete samples cA subjected to the DC test. The increase in porosity has the same trend as the results from open porosity measurements, see Fig. 5.4.

Label	Pores/cracks [%]	Other phases [%]
cA	2.82 ± 0.99	97.18 ± 0.99
cA-DC	4.60 ± 2.18	95.40 ± 2.18
increase [%]	1.78	-1.78

Table 5.12: Volume fraction of phases obtained from image analysis.

5.3.6 Thermogravimetric analysis and X-ray diffraction

For capacity and time reasons, both XRD and TGA experiments were performed only on the cA samples (see Fig. 5.3, set 3.). Simultaneous thermal analysis (STA), consisting of differential scanning calorimetry (DSC) and thermogravimetry (TG), was performed using a Labsys EVO TG/DSC from Setaram Inc. With a heating rate of 5 °C/min and the temperature range from 30 °C to 1000 °C were experiments done. During the measurements an argon atmosphere with a flow rate of 40 ml/min was set. XRD was performed using the powder diffraction technique using X-ray and it was done by PANalytical Aeris machine with Bragg-Brentano arrangement.

Thermogravimetric Analysis results

TG and DSC analysis revealed three distinct thermal decomposition processes. Firstly, the physically bound (PB) water and water bound chemically in C-S-H hydrates evolved between the ambient temperature and $\sim$250 °C. Portlandite $Ca(OH)_2$ decomposes between 450 and 500 °C and finally $CaCO_3$ polymorphs (calcite, aragonite, vaterite) between 610 and 800 °C. A decrease in PB water from C-S-H and gypsum was observed, which indicates that the passage of an electric current leaches these products from the cement matrix. The tangential method [107] determined the content of Portlandite and $CaCO_3$ polymorphs. The content of Portlandite in both samples is equal. Electrically non-treated sample cA contains 1.9% more calcite, see Tab. 5.13. This could mean, that due to the electric current treatment the calcite is also leaching out of the sample.

Label	PB water C-S-H, gypsum [%]	Portlandite* [%]	Calcite* [%]
cA	6.88	6.52	5.59
cA-DC	6.17	6.52	3.69
change [%]	-0.71	0.00	-1.90

Legend: *tangent method [107].

Table 5.13: Content of thermally-decomposed components (% by mass) where PB means physically bound.

X-Ray Diffraction results

The phase composition obtained by XRD is presented in Tab. 5.14. The system is very complicated due to the presence of mixed aggregates containing not only quartz but also many feldspar minerals (anorthite, oligoclase, albite, orthoclase), which are very similar and difficult to distinguish. The concrete contains a lot of C-S-H, which are amorphous and thus it is not indicated by XRD. Moreover, the concrete samples with coarse aggregates pose a risk of homogeneity and representativeness, so these results should be considered just as an indication. The content of calcite seems to be 2% higher for cA opposite sample cA-DC. Also tho content of portlandite is 2% higher for cA sample, which agrees with thermal analysis. This probably mean that all phases are leached out during the electric treatment of the samples, see Tab. 5.14.

Phase	Portlandite [%]	Calcite [%]	AFt [%]	AFm [%]
cA	9	6	2	3
cA-DC	7	4	1	4
change [%]	-2	-2	-1	1

Table 5.14: The phase composition in % obtained from XRD.

5.3.7 Comparison of porosity results after Direct Current Test from individual techniques

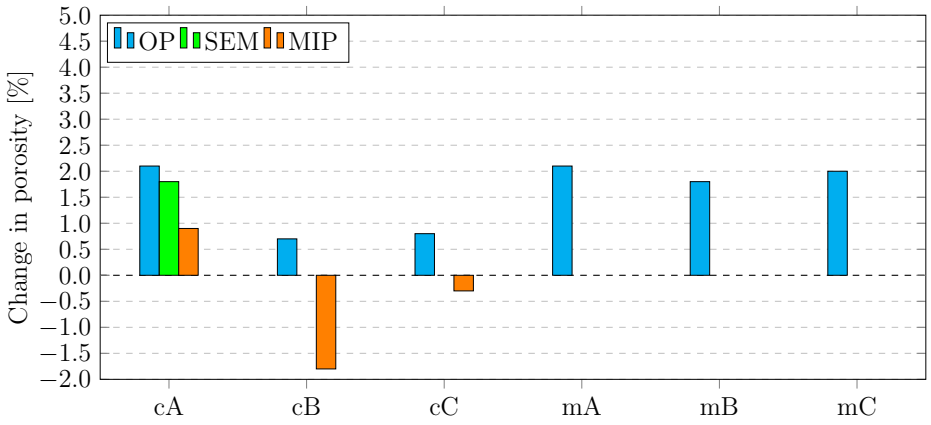

Figure 5.27: Absolute change in porosity for individual samples after different tests.

Label Change	cA [%]	cB [%]	cC [%]	mA [%]	mB [%]	mC [%]
OP	2.10	0.70	0.80	2.10	1.80	2.00
SEM	1.78	-	-	-	-	-
MIP	0.93	-1.78	-0.32	-	-	-

Table 5.15: Absolute change in porosity for individual samples after different tests.

Since each method has a different scope of operation (see Fig. 4.8), it is not appropriate to compare the following values with each other. While open porosity includes pores larger than 1 µm, SEM includes pores larger than 0.1 µm. MIP can detect pores between 0.004 um and 0.2 µm. The greatest increase in porosity was observed for the mixture of cA and mA, specifically, 2.10%. This means that the cA and mA mixture should be the most sensitive to the passage of electric current. The other methods, for capacity and time reasons, were carried out, as mentioned above, in a limited mode. The SEM results are only available for cA mixtures and MIP results are only available for concrete mixtures and are not available for mortar mixtures. However, an increase in porosity by 1.78% was found with the SEM method for the mixtures subjected to the DC test and an increase by 0.93% with the MIP method compared to the samples not subjected to the DC test. In addition, the MIP method showed an 1.78% decrease in porosity for the cB mixture and a 0.32% decrease in porosity for the cC mixture. This is most likely due to the fact that pores with detectable MIP dimensions have increased their porosity and moved outside the MIP detection range.

5.4 Conclusions from experimental part

Concrete and mortar samples were subjected to different types of tests from which results were obtained. The experiments were chosen so that the results obtained from them could be compared with each other and the trends obtained could be confirmed. However, the results of the experiments differ in some cases between the individual mixtures, but in principle the most important conclusions can be summarized in the following points:

- The porosity results show an increasing trend after the electric current passage for almost all techniques. The largest change in open porosity was observed for the cA and mA mixtures. In the case of porosity obtained by SEM and subsequent image analysis, an increase was recorded for the cA mixture also. The porosity obtained using the MIP technique does not follow a similar trend in the case of the cB and cC mixtures and a decrease in porosity was recorded after the electric current passage. However, this is probably due to the fact that pores with detectable MIP dimensions have increased their porosity and moved outside the detection range of the MIP technique.

- From the point of view of the influence of electricity on porosity, the best mixtures were cB and mB for which the smallest increase of porosity was recorded. They were followed by mixtures cC and mC and the worst were mixtures cA and mA. The reason why the greatest change has occurred in the mixtures cA and mA is that there has been no replacement of cement by admixtures. It can be concluded that it is the pure Portland cement matrix which is most prone to electric current passage. On the other hand, supplementary materials in blended cement are less vulnerable to the electric current passage. Also, fine admixtures as microsilica help to resist the adverse electric current effects.

- The total charge transported through the individual mixtures during ACPT was in all cases higher than during the DC test. This is despite the fact that the mobility of OH^- ions is higher than that of Cl^- ions. The increase in charge transfer during the ACPT test can be attributed to the fact that the ACPT was preceded by the DC test, which opened the porosity. The total charge transported through the individual mixtures during ACPT was also in all cases higher than during the NS test. This is an expected trend, since NS particles are much larger than Cl^- ions and therefore more difficult to pass through the porous system. The nanosilica particles also tend to aggregate and thus block transport. What is an expected and positive trend is that the total charge transported during ACPT in samples previously injected with NS was lower in all cases, except for

the cA mixture. In the experimental part it has been confirmed that the passage of electric current through concrete and mortar samples increases the porosity (see Fig. 5.4), which is also confirmed by several studies [34, 36, 104]. It can also be argued that the multiple passage of the electric current does not increase the porosity as significantly as the first passage, see Fig. 5.8.

- From the point of view of resistance to the passage of electric current, mixtures of cC and mC appear to be the most resistant. They are followed by mixtures cB and mB and the worst are again mixtures cA and mA. Again, from this it can be concluded that pure Portland cement mixtures resist the electric current passage the worst.

- The total amount of chloride increased for samples with longer ponding time, which is an expected trend. The effective diffusion coefficient increased for all mixtures after the DC test, what is the expected trend also. A similar trend did not occur with the chloride amount for the cA and cB mixture, where an increase in the amount was expected after the DC test. This is due to the lower surface concentration, which significantly reduced the total amount of chloride. In the case of the amount of chloride absorbed during natural diffusion, the mixtures cC were the best with the lowest amount (approximately half the amount of chloride recorded compared to cA). The samples cA, showed again the highest amount absorbed. The cB mixture was approximately in the middle. This confirms the above conclusions about resistance and susceptibility to electric current passage.

- The results of the NS injection effectiveness were not as expected. After NS injection, the diffusion coefficient of the cB mixture increased by 946%. It was also expected that the total amount of chloride after NS injection would be lower than in the case of samples subjected to the DC test or in the case of samples not subjected to the any electrical test. In the case of the cC mixture, an overall increase in chloride content of up to 152% was recorded after NS injection. However, a decreased surface chloride concentration was recorded for almost all mixtures after NS injection, which is a positive trend. The best performance in NS injection appears to be cB followed by cC. The worst appears to be cA. It is important to recall that the amount of chloride increased in all cases after NS injection, which suggests that the effect of electric current treatment is superior to the positive effect of nanosilica treatments. This hypothesis would more in-depth investigation.

- Both TGA and XRD analysis recorded that the passage of an electric current causes volumetric decrease of calcite in the concrete mixture cA. A decrease in PB water from C-S-H and gypsum was also observed using the TGA technique,

which could indicate that the passage of an electric current leaches these products from the cement matrix. The Portlandite content remained unchanged, see Tab. 5.13. On the contrary, a decrease in Portlandite was observed in the XRD results. However, the XRD technique does not identify C-S-H, which represents a significant volume of the cement paste and thus makes the other changes less recognizable.

6 Model and numerical results

Numerical models have been constructed for different types of tests, which include the theoretical chloride transfer. Chloride transfer can be natural or accelerated by an electric current. As a simplification, no binding is assumed and effective diffusion characteristics prescribed. The models are used to validate experimental trends and calculate theoretical chloride profiles where the experimental data are not available.

6.1 Pure diffusion problem

The Nernst-Planck equation can be, in one dimensional case, written as:

$$\frac{dC}{dt} = D.\left(\frac{d^2C}{dx^2} + \frac{zF}{RT}.\frac{dC}{dx}.\frac{d\Phi}{dx}\right). \tag{6.1}$$

In the case of natural diffusion, the electric potential is zero and the solution can be simplified to the following equation, which is actually the second Fick's law:

$$\frac{dC}{dt} = D.\frac{d^2C}{dx^2}, \tag{6.2}$$

Numerical solution of Eq. 6.2 may employ the central finite difference approximation with $x \in <0; l>$ and $t \in <0; T>$. In case we divide l into n intervals of $\Delta x = \frac{l}{n}$ the following finite difference scheme for the derivatives is:

$$\frac{dC(x,t)}{dx} \approx \frac{C(x_{\text{i+1}},t) - C(x_{\text{i-1}},t)}{2\Delta x}, \tag{6.3}$$

$$\frac{d^2C(x,t)}{dx^2} \approx \frac{C(x_{\text{i-1}},t) - 2C(x_{\text{i}},t) + C(x_{\text{i+1}},t)}{(\Delta x)^2}. \tag{6.4}$$

By minimizing the least square error between the experimental results and the analytical solution (see Eq. 4.10), the effective diffusion coefficient D_{eff} and surface chloride concentration C_{s} were estimated, see Tab. 5.7. These values were also used as material parameter and boundary condition in the central difference solution.

The numerical solution was implemented to python code, which can be seen in Appendix 2, see Chapter 8. The numerical parameters, i.e. diffusion coefficient and surface concentration, were taken from the analytical solution and their values can be seen in Tab. 5.7.

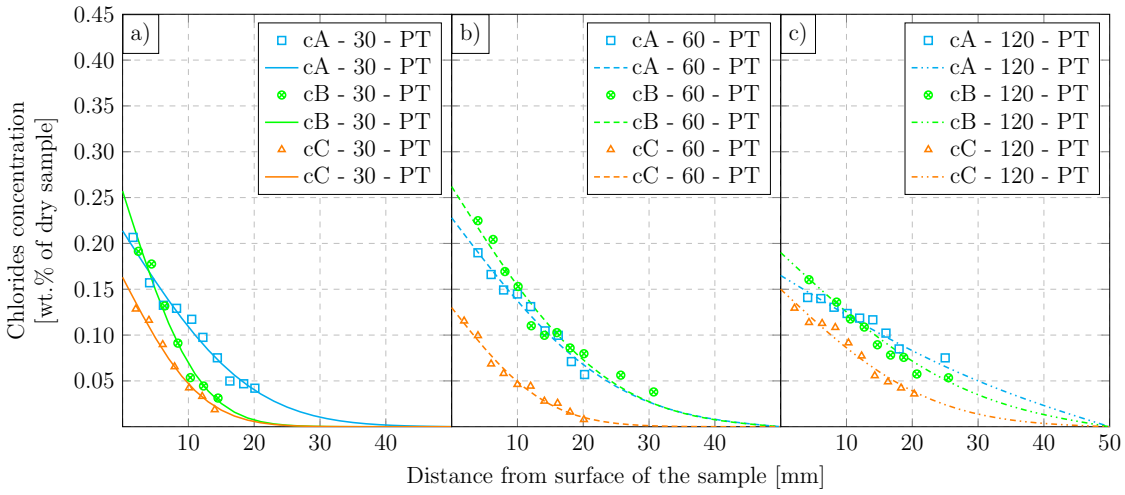

Figure 6.1: Experimental (marks) and numerical (curves) results comparison of chloride concentrations for a) 30, b) 60 and c) 120 days after ponding test.

The numerical and analytical solution (see Eq. 4.10), was identical in almost all cases. Smaller deviations were observed for samples after the ponding test for 120 days, where the chloride concentration on the other, non-chloride-exposed side of the sample was greater than zero. The difference can be observed in Fig. 6.2, where it can be seen that the numerical solution in all cases led to a zero concentration on the other side of the sample. This is because in the case of the numerical solution, the zero at a distance of 50 mm is prescribed by boundary conditions. In the case of the analytical solution, zero concentration is prescribed in infinity. In Fig. 6.2, it is possible to observe a small difference between the mixtures cA and cB at a distance of 50 mm. By these comparisons, the numerical solution (see Eq. 6.3) was verified to be equivalent to the analytical one (see Eq. 4.10).

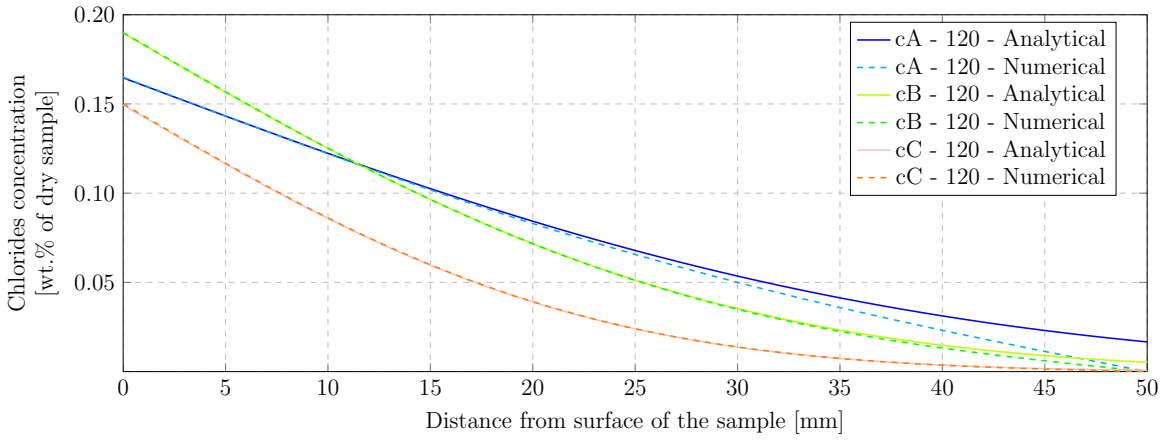

Figure 6.2: Analytical vs numerical results for 120 days chloride exposed samples.

6.2 Diffusion-convection problem with positive flux (chloride penetration)

This model describes the situation of chloride penetration to the sample from one side accelerated by an electric field (ACPT), see Eq. 6.1. For numerical solution of Eq. 6.1 backward differences can be used. In this case, the first derivative is defined as:

$$\frac{dC(x,t)}{dx} \approx \frac{C(x_{\mathrm{i}},t) - C(x_{\mathrm{i-1}},t)}{\Delta x}. \tag{6.5}$$

The numerical solution was also implemented to python code and can be seen in Appendix 3, see Chapter 8. The surface concetration C_{s} at one side and zero concentration at the other side of the sample were prescribed as boundary conditions. Material parameter was the effective diffusion coefficient D_{eff}. Both values were taken from the results of the analytical solution so that the results from the models could be compared with each other. The selected values can be seen in the Tab. 5.7. It should be reminded that the times of 30, 60 and 120 days apply only to samples that have been subjected to a ponding test. As the effective diffusion coefficient and surface chloride concentration evaluated from ponding tests differ, the results have been made for all these values in order to be able to make a valid comparison.

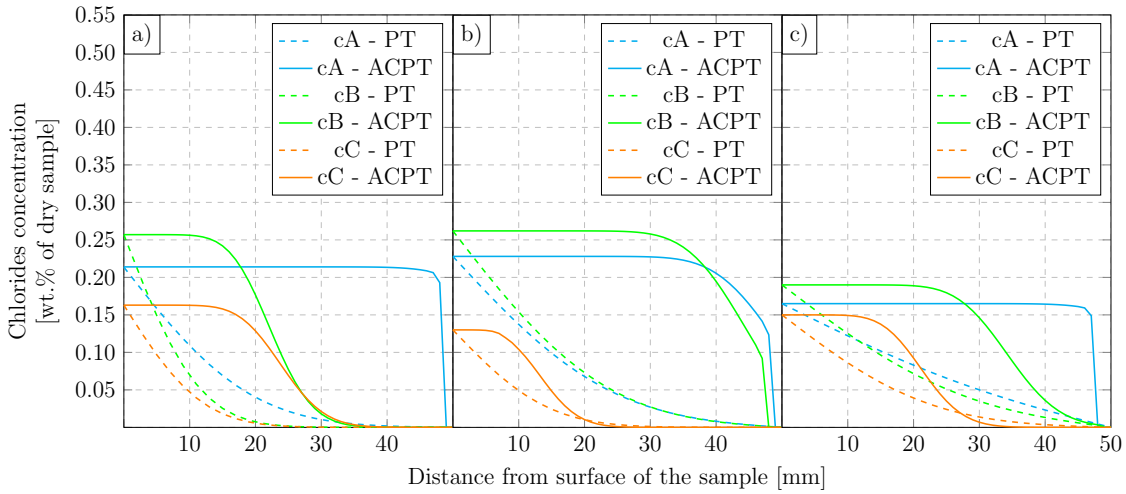

Figure 6.3: Numerical results comparison of the PT and ACPT for set of parameters a) 30, b) 60 and c) 120 days obtained from analytical solution of PT.

In the accelerated test the profile is convective, i.e. step decrease, while in the diffusion test there is a gradual decrease in concentration according to the error function. The ACPT numerical model is a combination of both with much higher influence of the convective process. It is possible to see it in Fig. 6.3, where the highest concentration value at any depth is maximally equal to the surface chloride concentration. There is

also no step decrease in chloride concentration because of the influence of diffusion. In cases where the diffusion coefficient is higher, especially for the cA mixture, it can be seen that the chlorides have been pushed through almost the entire sample during the 24 hours duration of the 20 V electric voltage test.

The numerical model also showed that for the same parameters of individual mixtures, ACPT is much more effective in chloride penetration than ponding test. It is also important to note that both models do not include chloride binding. The greatest increase in chloride amount after the ACPT test was again observed for the cA mixture, which confirms other results. With the parameters from the ponding test, which lasted 30 days, an increase of 297% was recorded for the cA mixture. The smallest increase of 52% was recorded for the cC mixture when the parameters from the 60 and 120 day ponding tests were taken. The chloride amount for both models is summarized in Tab. 6.1.

set of parameters	"30"			"60"			"120"		
Samples	cA	cB	cC	cA	cB	cC	cA	cB	cC
PT w_{Cl} [g]	45.0	32.4	21.3	60.0	66.4	20.4	65.6	58.7	36.7
ACPT w_{Cl} [g]	178.7	95.0	68.2	181.3	195.0	31.0	134.9	113.7	55.9
Change [%]	297	210	220	202	193	52	106	94	52

Legend: set of parameters from analytical results of PT for exposure times in quotes.

Table 6.1: Total amount of chlorides evaluated from PT and ACPT from numerical model results.

The total amount of chloride was generally highest in the cA mixture, which is consistent with the results from the open porosity and also with the results from the ponding test. However, the largest amount of chloride was in mixture cB, specifically 195 g. This is most likely an error, because all other results show decreases in the mixture of cB and cC compared to the mixture of cA. On the other hand, the cC mixtures showed overall the smallest amount of chlorides and appeared to be the most resistant.

From the comparison made between PT and ACPT (see Fig. 6.3), it can be concluded that during the ACPT period (24 hours), chlorides travel further compared to PT, which was carried out for 30, 60 and 120 days. This shows significant speed-up of chloride migration.

7 Conclusions

In this thesis a combination of techniques have been used and several types of mixtures have been studied, which makes it reasonable to summarize the work into general conclusions:

- Almost all techniques used to determine porosity recorded an increase after passage of an electric current. The largest increase in open porosity was found for the cA concrete mixture and the mA mortar mixture. Concrete mixture cA was made from Portland cement CEM I 42.5R with coefficient w/b = 0.8. Mortar mix mA was made from the same components, except aggregate 4 - 16 mm. In the case of the mixture cB and mB, CEM I 42.5R was replaced by the same mass of cement CEM II/A-M(LL) 42.5R. In the mixture cC and mC, 10% of the CEM I 42.5R was replaced by microsilica. For cB, cC, mB and mC, the increase in open porosity of these mixtures is similar but smaller than in the mixtures cA and mA. The results obtained from MIP show decrease in porosity after electric current passage for mixtures cB and cC. This means that the size of the pores has been increased. In case of the cA sample increase in porosity detected by MIP was recorded. However, it is important to note, that the MIP technique does not operate in the same interval of pores as the other methods.

- In all cases, there was also an increase in the total transported charge during the ACPT test compared to the DC test, despite the fact that the mobility of OH^- ions is higher than that of Cl^- ions. The increase in transported charge during the ACPT compared to the DC test can be attributed to the fact that the ACPT test followed the DC test, which increased the porosity and thus allowed an augmented effect after the ACPT test.

- During the NS test, the total charge was in all cases the smallest and this is due to the fact that nanosilica particles are much larger than OH^- and Cl^- ions and therefore it is more difficult for them to pass through the same pore system. Another big reason was the decrease in the amount of charge that NS carries. In suspension, the electrical charge of NS particles influences their colloidal stability and a decrease in the charge leading to particle aggregation. The nanosilica particles also tend to aggregate on the surface of the penetrated part of the sample, which caused an increased resistivity and thus a decreased electric current. However, a decrease in total current was observed in the ACPT test that followed the NS injection test, compared to the ACPT test that followed the DC test, which is a positive trend.

- The results of the chloride profiles showed higher chloride amount in samples that had been in solution for longer periods of time during the ponding test, which was expected trend. Chloride profiles shown an decrease in the total chloride amount in the samples cA and cB after electric current passage. In this case it was probably a measurement error, since their effective diffusion coefficient was increased after passing through the electric current. The lower amount of chloride was calculated due to the low surface concentration. In the case of the cC mixture there was recorded an increase in porosity after DC test, which is the expected trend. There was also recorded an increase in chloride amount in the samples that were previously treated with nanosilica and were expected to have a higher resistance to chlorides. This trend is inconsistent with the results of the overall charge. This means that the nanosilica probably clogs the pores on the surface, but disrupts the microstructure inside of the sample.

- Both XRD and TGA methods confirm that the passage of an electric current causes the hydration products and calcite to leach. These results have been carried out only on cA mixtures due to time and capacity reasons.

- The same results have been obtained from numerical and analytical solutions of the diffusion process when using the same set of parameters. A numerical model for accelerated chloride penetration has also been developed, which shows a significantly higher total chloride amount than in samples that have been penetrated with chlorides naturally. The model well describes the differences between the accelerated and natural processes although some phenomena like binding were not considered in the modeling.

- In terms of chloride resistance, cB appears to be the most suitable mixture. Although, mixture cC resisted similarly. The worst results were recorded for the cA mixture where the chloride penetration was, in general, the easiest. The suitability of NS injection is debatable, since in all cases an increase in chloride amount was recorded after NS injection. However, the smallest increase was recorded for the cB mixture, followed closely by the cC mixture. The largest increase in chloride amount after NS injection was recorded in the cA mixture, which was twice as high as in the cC mixture. Positive effect of NS treatment can be found in the decrease of surface chloride concentration.

It is also important to note that the conditions under which the electromigration techniques were applied in this work may not perfectly simulate actual field conditions. The variability of concrete properties, environmental factors, and others in real structures could significantly affect the effectiveness of these techniques.

Future outlook

On the basis of the results of this thesis and on the basis of observations from this topic, it would be appropriate to investigate in the future:

- Invent a better and automatic grinding of the layers for the following titration, from which the chloride profile is then determined. This is not only for time reasons, but also for accuracy reasons. Also to process in this way a considerably larger number of samples, in order to confirm or deny the samples more clearly and to detect possible errors. This was in the experimental plan, but for time reasons it was not possible to implement.
- Perform XRD,TGA measurements and SEM with following image analysis on the other mixtures and see if the other mixtures behave the same way and confirm the results if necessary.
- To implement a system of nanosilica mixing that would prevent, or at least slow down, the aggregation of particles and thereby delay the time when a barrier of aggregates is formed on the surface, which acts as a blocking factor to further penetration.
- Generate a larger statistics of the data to confirm or disprove the conclusions that were made upon limited number of experiments.

Bibliography

[1] C. R. Gagg. Cement and concrete as an engineering material: An historic appraisal and case study analysis. *Engineering Failure Analysis*, 40:114–140, 2014.

[2] R. Loser, B. Lothenbach, A. Leemann, and M. Tuchschmid. Chloride resistance of concrete and its binding capacity – comparison between experimental results and thermodynamic modeling. *Cement and Concrete Composites*, 32(1):34–42, 2010.

[3] A. Guettala and A. Abibsi. Corrosion degradation and repair of a concrete bridge. *Materials and Structures/Materiaux et Constructions*, 39(288):471 – 478, 2006. Cited by: 12.

[4] J. Němeček, L. Li, and Y. Xi. Electrokinetic nanoparticle injection for remediating leaks in oil well cement. *Construction and Building Materials*, 156:63–72, 2017.

[5] J. Němeček, J. Kruis, T. Koudelka, and T. Krejčí. Simulation of chloride migration in reinforced concrete. *Applied Mathematics and Computation*, 319:575–585, 2018. Recent Advances in Computing.

[6] J. Němeček, R. Šulc, J. Němečková, and J. Kruis. Nanoparticles in concrete: Application in fresh and hardened state. *Key Engineering Materials*, 760:3–9, 01 2018.

[7] N. Jafariesfad, M. Geiker, S. Sangesland, K. Gawel, and M. Torsæter. Electrokinetics application in concrete and well construction. 08 2020.

[8] S. Sawada, C. Page, and M. Page. Electrochemical injection of organic corrosion inhibitors into concrete. *Corrosion Science*, 47(8):2063–2078, 2005.

[9] C. ASTM et al. Standard test method for electrical indication of concrete's ability to resist chloride ion penetration. *C1202–18*, 2012.

[10] K.-S. Huang and C.-C. Yang. Using rcpt determine the migration coefficient to assess the durability of concrete. *Construction and Building Materials*, 167: 822–830, 2018.

[11] S. Safarzadegan Gilan, H. Bahrami Jovein, and A. A. Ramezanianpour. Hybrid support vector regression – particle swarm optimization for prediction of compressive strength and rcpt of concretes containing metakaolin. *Construction and Building Materials*, 34:321–329, 2012.

[12] P. A. G. Jemimah Carmichael. M. Rapid chloride permeability test on concrete with nano materials. *International Journal of Engineering and Advanced Technology (IJEAT)*, 8, February 2019.

[13] A. Susanto, D. A. Koleva, K. van Breugel, and K. van Beek. Stray current-induced development of cement-based microstructure in water-submerged, ca

(oh) 2-submerged and sealed conditions. *Journal of Advanced Concrete Technology*, 15(6):244–268, 2017.

[14] M. Siegwart, J. F. Lyness, and B. J. McFarland. Change of pore size in concrete due to electrochemical chloride extraction and possible implications for the migration of ions. *Cement and Concrete Research*, 33(8):1211–1221, 2003.

[15] S. Kawashima, P. Hou, D. J. Corr, and S. P. Shah. Modification of cement-based materials with nanoparticles. *Cement and Concrete Composites*, 36:8–15, 2013. Special issue: Nanotechnology in Construction.

[16] F. Sanchez and K. Sobolev. Nanotechnology in concrete – a review. *Construction and Building Materials*, 24(11):2060 – 2071, 2010.

[17] D. R. Vieira, A. L. R. Moreira, J. L. Calmon, and W. K. Dominicini. Service life modeling of a bridge in a tropical marine environment for durable design. *Construction and Building Materials*, 163:315–325, 2018.

[18] T. H. Y. Nguyen, V. M. Tran, W. Pansuk, N. T. Cao, and V. H. L. Bui. Electrochemical chloride extraction on reinforced concrete contaminated external chloride: Efficiencies of intermittent applications and impacts on hydration products. *Cement and Concrete Composites*, 121:104076, 2021.

[19] T. Luping and L.-O. Nilsson. Chloride binding capacity and binding isotherms of opc pastes and mortars. *Cement and Concrete Research*, 23(2):247–253, 1993.

[20] D. Li, L. yuan Li, and X. Wang. Chloride diffusion model for concrete in marine environment with considering binding effect. *Marine Structures*, 66:44–51, 2019.

[21] R. Gabrovšek, T. Vuk, and V. Kaučič. Evaluation of the hydration of portland cement containing various carbonates by means of thermal analysis. *Acta Chimica Slovenica*, 53, 01 2006.

[22] R. Capozucca. Damage to reinforced concrete due to reinforcement corrosion. *Construction and Building Materials*, 9(5):295–303, 1995.

[23] S. Y. Jang, B. S. Kim, and B. H. Oh. Effect of crack width on chloride diffusion coefficients of concrete by steady-state migration tests. *Cement and Concrete Research*, 41(1):9–19, 2011.

[24] I.-S. Yoon, E. Schlangen, M. de Rooij, and K. Breugel. The effect of cracks on chloride penetration into concrete. *Key Engineering Materials - KEY ENG MAT*, 348-349:769–772, 09 2007.

[25] W. Li, W. Liu, and S. Wang. The effect of crack width on chloride-induced corrosion of steel in concrete. *Advances in Materials Science and Engineering*, 2017:1–11, 07 2017.

[26] A. Khitab, M. Arshad, S. Ali, S. Kazmi, and M. Munir. Modeling of chloride ingress in concrete using fick's laws: Review and historical perspective. *Science International*, 26:1519–1521, 09 2014.

[27] C. Chiang and C. Yang. Relation between the diffusion characteristic of concrete from salt ponding test and accelerated chloride migration test. *Materials Chemistry and Physics*, 106(2):240–246, 2007.

[28] C. Hall. Water sorptivity of mortars and concretes: a review. *Magazine of Concrete Research*, 41:51–61, 1989.

[29] T. J. M. Alfatlawi and R. A. A. Alsultani. Characterization of chloride penetration in hydraulic concrete structures exposed to different heads of seawater: Using hydraulic pressure tank. *Engineering Science and Technology, an International Journal*, 22(3):939–946, 2019.

[30] H. Liu and X. Yang. Effect of hydrostatic pressure on chloride ion transport behavior in concrete, 2022. Cited by: 0.

[31] H. Wu and L.-m. HU. Experimental study on electro-osmotic consolidation of expansive soils. pages 4060–4068, 03 2012.

[32] F. Bjork, B. Sederholm, J. Trägårdh, and B. Olofsson. Electroosmosis – a method applied for handling of moisture in foundations. *E3S Web of Conferences*, 172: 17010, 01 2020.

[33] J. Němeček and Y. Xi. *Electrochemical Injection of Nanoparticles into Existing Reinforced Concrete Structures*. 2015.

[34] J. J. Thomas and H. M. Jennings. Materials of cement science primer: The science of concrete. 2009.

[35] L. R. de Almeida Souza, M. H. F. de Medeiros, E. Pereira, and A. P. B. Capraro. Electrochemical chloride extraction: Efficiency and impact on concrete containing 1 *Construction and Building Materials*, 145:435–444, 2017.

[36] H. Chu, B. Zhang, S. Zhao, M. Guo, Y. Liang, L. Jiang, and Z. Song. Effect of electric current on the stability of bound chloride. *Cement and Concrete Composites*, 103:71–79, 2019.

[37] G. H. Barbhuiya, M. A. Moiz, S. D. Hasan, and M. M. Zaheer. Effects of the nanosilica addition on cement concrete: A review. *Materials Today: Proceedings*, 32:560–566, 2020. 3rd International Conference on Innovative Technologies for Clean and Sustainable Development.

[38] A. P. P., D. K. Nayak, B. Sangoju, R. Kumar, and V. Kumar. Effect of nanosilica in concrete; a review. *Construction and Building Materials*, 278:122347, 2021.

[39] H. F. Taylor. *Cement chemistry*. Thomas Telford, 1997.

[40] G. DeBruijn and S. M. Whitton. Chapter five - fluids. In G. Liu, editor, *Applied Well Cementing Engineering*, pages 163–251. Gulf Professional Publishing, 2021.

[41] K. De Weerdt, M. B. Haha, G. Le Saout, K. Kjellsen, H. Justnes, and B. Lothenbach. Hydration mechanisms of ternary portland cements containing limestone powder and fly ash. *Cement and Concrete Research*, 41(3):279–291, 2011.

[42] R. Kurihara and I. Maruyama. Revisiting tennis-jennings method to quantify low-density/high-density calcium silicate hydrates in portland cement pastes. *Cement and Concrete Research*, 156:106786, 2022.

[43] S. Diamond. The microstructure of cement paste and concrete—-a visual primer. *Cement and Concrete Composites*, 26(8):919–933, 2004. Scanning electron microscopy of cements and concretes.

[44] *EN 197-1:2011, Cement - Část 1: Složení, specifikace a kritéria shody cementů pro obecné použití*. European Committee for Standardization, 1997.

[45] H. M. Jennings. Refinements to colloid model of c-s-h in cement: Cm-ii. *Cement and Concrete Research*, 38(3):275–289, 2008.

[46] W. Liao, X. Sun, A. Kumar, H. Sun, and H. Ma. Hydration of binary portland cement blends containing silica fume: A decoupling method to estimate degrees of hydration and pozzolanic reaction. *Frontiers in Materials*, 6, 2019.

[47] T. C. Hansen. Physical structure of hardened cement paste. a classical approach. *Materials and Structures*, 19(6):423–436, 1986.

[48] T. C. Powers and T. L. Brownyard. Studies of the physical properties of hardened portland cement paste. 1946.

[49] F.-J. Ulm, M. Abuhaikal, T. Petersen, and R. Pellenq. Poro-chemo-fracture-mechanics ... bottom-up: Application to risk of fracture design of oil and gas cement sheath at early ages. *Computational Modelling of Concrete Structures - Proceedings of EURO-C 2014*, 1:61–71, 01 2014.

[50] S. Mindess, J. Young, and D. Darwin. *Concrete*. Prentice-Hall civil engineering and engineering mechanics series. Prentice Hall, 2003.

[51] V. Kocaba. Development and evaluation of methods to follow microstructural development of cementitious systems including slags. 01 2009.

[52] I. Pane and W. Hansen. Investigation of blended cement hydration by isothermal calorimetry and thermal analysis. *Cement and Concrete Research*, 35(6):1155–1164, 2005.

[53] H. Zhang, Y. Xu, Y. Gan, Z. Chang, E. Schlangen, and B. Šavija. Microstructure informed micromechanical modelling of hydrated cement paste: Techniques and challenges. *Construction and Building Materials*, 251:118983, 2020.

[54] D. P. Bentz. Cemhyd3d: A three-dimensional cement hydration and microstructure development modeling package, version 3.0.

[55] K. van Breugel. Simulation of hydration and formation of structure in hardening cement-based materials. 1991.

[56] V. Šmilauer and Z. Bittnar. Microstructure-based micromechanical prediction of elastic properties in hydrating cement paste. *Cement and Concrete Research*, 36 (9):1708 – 1718, 2006.

[57] A. W. Coats and J. P. Redfern. Thermogravimetric analysis. a review. *Analyst*, 88:906–924, 1963.

[58] L. M. Ottosen, I. V. Christensen, I. Rörig-Dalgård, P. E. Jensen, and H. K. Hansen. Utilization of electromigration in civil and environmental engineering—processes, transport rates and matrix changes. *Journal of Environmental Science and Health, Part A*, 43(8):795–809, 2008.

[59] S. Lim and P. Mondal. Micro- and nano-scale characterization to study the thermal degradation of cement-based materials. *Materials Characterization*, 92: 15–25, 2014.

[60] P. Mehta and P. Monteiro. *Concrete : Microstructure, Properties, and Materials: Microstructure, Properties, and Materials*. McGraw Hill professional. Mcgraw-hill, 2005.

[61] K. L. Scrivener, P. Juilland, and P. J. Monteiro. Advances in understanding hydration of portland cement. *Cement and Concrete Research*, 78:38–56, 2015. Keynote papers from 14th International Congress on the Chemistry of Cement (ICCC 2015).

[62] S. Nasrazadani and S. Hassani. Chapter 2 - modern analytical techniques in failure analysis of aerospace, chemical, and oil and gas industries. In A. S. H. Makhlouf and M. Aliofkhazraei, editors, *Handbook of Materials Failure Analysis with Case Studies from the Oil and Gas Industry*, pages 39–54. Butterworth-Heinemann, 2016.

[63] C. Kittel. *Introduction to solid state physics*. John Wiley & Sons, Nashville, TN, 5 edition, January 1976.

[64] F. Kontoleontos, P. Tsakiridis, A. Marinos, N. Katsiotis, V. Kaloidas, and M. Katsioti. Dry-grinded ultrafine cements hydration. physicochemical and microstructural characterization. *Materials Research*, 16:404–416, 04 2013.

[65] L. Reimer, P. Hawkes, A. Schawlow, K. Shimoda, A. Siegman, and T. Tamir. *Scanning Electron Microscopy: Physics of Image Formation and Microanalysis*. Springer Series in Optical Sciences. Springer, 1998.

[66] A. Luis, L. Deng, L. Shao, and H. A. Li. Triaxial behaviour and image analysis of edmonton clay treated with cement and fly ash. *Construction and Building Materials*, 197:208–219, 2019.

[67] N. Otsu. A threshold selection method from gray-level histograms. *IEEE transactions on systems, man, and cybernetics*, 9(1):62–66, 1979.

[68] F. Rostasy, R. Weiss, and G. Wiedemann. Changes of pore structure of cement mortars due to temperature. *Cement and Concrete Research*, 10(2):157–164, 1980.

[69] R. Šulc, M. Himmel, and J. Němeček. Chloride resistance of concrete with fly ash. *AIP Conference Proceedings*, 2210(1):020010, 2020.

[70] L. Anovitz and D. Cole. Characterization and analysis of porosity and pore structures. *Reviews in Mineralogy and Geochemistry*, 80:61–164, 01 2015.

[71] I. Soroka. *Portland cement paste and concrete*. Macmillan International Higher Education, 1979.

[72] K. Newman. Concrete systems. *Composite materials*, pages 336–452, 1966.

[73] Y. Peng, L. Su, Y. Wang, and L. Zhang. Analysis of the effect of porosity in concrete under compression based on dip technology. *Journal of Materials in Civil Engineering*, 34, 01 2022.

[74] A. Aili and I. Maruyama. Review of several experimental methods for characterization of micro-and nano-scale pores in cement-based material. *International Journal of Concrete Structures and Materials*, 14(1):1–18, 2020.

[75] A. Abell, K. Willis, and D. Lange. Mercury intrusion porosimetry and image analysis of cement-based materials. *Journal of Colloid and Interface Science*, 211(1):39–44, 1999.

[76] C. Voigt, J. Hubálková, H. Giesche, and C. G. Aneziris. Intrusion and extrusion mercury porosimetry measurements at al2o3–c - influence of measuring parameter. *Microporous and Mesoporous Materials*, 299:110125, 2020.

[77] J. Zhou, G. Ye, and K. van Breugel. Characterization of pore structure in cement-based materials using pressurization–depressurization cycling mercury intrusion porosimetry (pdc-mip). *Cement and Concrete Research*, 40(7):1120–1128, 2010.

[78] M. Staněk and Y. Géraud. Granite micro-porosity changes due to fracturing and alteration: secondary mineral phases as proxies for porosity and permeability estimation. *Solid Earth Discussions*, pages 1–38, 10 2018.

[79] S. P. Rigby, D. Barwick, R. S. Fletcher, and S. N. Riley. Interpreting mercury porosimetry data for catalyst supports using semi-empirical alternatives to the washburn equation. *Applied Catalysis A: General*, 238(2):303–318, 2003.

[80] N. Nestle, P. Galvosas, and J. Kärger. Liquid-phase self-diffusion in hydrating cement pastes—results from nmr studies and perspectives for further research. *Cement and concrete research*, 37(3):398–413, 2007.

[81] G. Song. Equivalent circuit model for ac electrochemical impedance spectroscopy of concrete. *Cement and Concrete Research*, 30(11):1723–1730, 2000.

[82] A. Ruiz, H. Hernández, J. Hernández, R. Orozco-Cruz, A. Ruiz Reynoso, C. González, and J. Miranda-Hernández. *Electrochemical Impedance Spectroscopy (EIS): A Review Study of Basic Aspects of the Corrosion Mechanism Applied to Steels*. 11 2020.

[83] I. Sánchez, X. Nóvoa, G. de Vera, and M. Climent. Microstructural modifications in portland cement concrete due to forced ionic migration tests. study by impedance spectroscopy. *Cement and Concrete Research*, 38(7):1015–1025, 2008.

[84] H.-W. Song, C.-H. Lee, and K. Y. Ann. Factors influencing chloride transport in concrete structures exposed to marine environments. *Cement and Concrete Composites*, 30(2):113–121, 2008.

[85] M. Medeiros, J. H. Filho, and P. Helene. Influence of the slice position on chloride migration tests for concrete in marine conditions. *Marine Structures*, 22(2):128–141, 2009.

[86] N. Buenfeld, M. Shurafa-Daoudi, and I. McLoughlin. Chloride transport due to wick action in concrete', in'chloride penetration into concrete'. In *Proceedings of RILEM International Workshop on Chloride Penetration into Concrete, Nilsson L.-O. and Ollivier JP eds.(RILEM Publications, Paris, 1996)*, pages 302–324, 1995.

[87] J. Crank. *The mathematics of diffusion*. Oxford university press, 1979.

[88] X. Ke, S. Bernal, O. Hussein, and J. Provis. Chloride binding and mobility in sodium carbonate-activated slag pastes and mortars. *Materials and Structures*, 50, 12 2017.

[89] M. Tsui Chang, C. Qiao, L. Montanari, P. Suraneni, and W. Weiss. Chloride binding of cementitious materials exposed to sodium chloride using x-ray fluorescence. *Aci Materials Journal*, 116, 09 2019.

[90] A. Delagrave, J. Marchand, J.-P. Ollivier, S. Julien, and K. Hazrati. Chloride binding capacity of various hydrated cement paste systems. *Advanced Cement Based Materials*, 6(1):28–35, 1997.

[91] Z. Liu, Y. Wang, J. Wang, C. Liu, J. Jiang, and H. Li. Experiment and simulation of chloride ion transport and binding in concrete under the coupling of diffusion and convection. *Journal of Building Engineering*, 45:103610, 2022.

[92] M. Thomas, R. Hooton, A. Scott, and H. Zibara. The effect of supplementary cementitious materials on chloride binding in hardened cement paste. *Cement and Concrete Research*, 42(1):1–7, 2012.

[93] A. Squillace, W. Li, W. Liu, and S. Wang. The effect of crack width on chloride-induced corrosion of steel in concrete. *Advances in Materials Science and Engineering*, 2017:3968578, 2017.

[94] S. Jang, B. Kim, and B. Oh. Effect of crack width on chloride diffusion coefficients of concrete by steady-state migration tests. *Cement and Concrete Research - CEM CONCR RES*, 41:9–19, 01 2011.

[95] A. Dousti, R. Rashetnia, B. Ahmadi, and M. Shekarchi. Influence of exposure temperature on chloride diffusion in concretes incorporating silica fume or natural zeolite. *Construction and Building Materials*, 49:393–399, 2013.

[96] M. Hisada, S. Nagataki, and N. Otsuki. Evaluation of mineral admixtures on the viewpoint of chloride ion migration through mortar. *Cement and Concrete Composites*, 21(5):443–448, 1999.

[97] A. Ramezanianpour, H. Rezaei, and H. Savoj. Influence of silica fume on chloride diffusion and corrosion resistance of concrete - a review. *Asian Journal of Civil Engineering*, 16:301–321, 09 2014.

[98] J. Varcoe, P. Atanassov, D. Dekel, A. Herring, M. Hickner, P. Kohl, A. Kucernak, W. Mustain, K. Nijmeijer, K. Scott, T. Xu, and L. Zhuang. Anion-exchange membranes in electrochemical energy systems. *Energy Environ. Sci.*, 7:3135, 08 2014.

[99] A. Regberg, K. Singha, M. Tien, F. Picardal, Q. Zheng, J. Schieber, E. Roden, S. Brantley, and C. Regberg. Electrical conductivity as an indicator of iron reduction rates in abiotic and biotic systems. *Water Resources Research - WATER RESOUR RES*, 47, 04 2011.

[100] G. Mays. *Durability of Concrete Structures: Investigation, repair, protection.* CRC Press, 1991.

[101] C. Andrade, C. Alonso, J. Gulikers, R. Polder, R. Cigna, Ø. Vennesland, M. Salta, A. Raharinaivo, and B. Elsener. Test methods for on-site corrosion rate measurement of steel reinforcement in concrete by means of the polarization resistance method. *Materials and Structures/Materiaux et Constructions*, 37:623–643, 11 2004.

[102] T. Luping and L.-O. Nilsson. Rapid determination of the chloride diffusivity in concrete by applying an electric field. *Materials*, 89:49–53, 1993.

[103] R. Thomas, E. Ariyachandra, D. Lezama, and S. Peethamparan. Comparison of chloride permeability methods for alkali-activated concrete. *Construction and Building Materials*, 165:104–111, 2018.

[104] L. Zheng, M. Jones, and Z. Song. Concrete pore structure and performance changes due to the electrical chloride penetration and extraction. *Journal of Sustainable Cement-Based Materials*, 5:1–15, 10 2015.

[105] T. H. Y. Nguyen, H. Yokota, and K. Hashimoto. Effects of electrochemical chloride extraction on hydrated products of various cement paste systems. *Journal of Advanced Concrete Technology*, 13:564–582, 12 2015.

[106] J. Němeček, J. Lukeš, and J. Němeček. High-speed mechanical mapping of blended cement pastes and its comparison with standard modes of nanoindentation. *Materials Today Communications*, 23:100806, 2020.

[107] K. Scrivener, R. Snellings, B. Lothenbach, et al. *A practical guide to microstructural analysis of cementitious materials*, volume 540. Crc Press Boca Raton, FL, USA:, 2016.

8 Appendix

8.1 Appendix 1

```
import numpy as np
from scipy import special, optimize
import math

def fitting_fun(x, conc, diff):
    concentration_result = conc * (1 - (special.erf(x/(2*math.sqrt(abs(diff*t))))))  #equation
    return concentration_result

x_data = [0.0020,0.0050,0.0065,0.0215,0.0265].  #x depth data
y_data = [0.158,0.143,0.134,0.059,0.043]        #y chloride concentration data
x_data = np.asarray(x_data)
y_data = np.asarray(y_data)
t = 2592000
p0 = 0.1, 0.000000001                           #starting values

params, cov = optimize.curve_fit(fitting_fun, x_data, y_data, p0)
fitC = params[0]
fitDiff = abs(params[1])

print(fitC)     #print parameter C
print(fitDiff)  #print parameter D
```

8.2 Appendix 2

```
import numpy as np
import matplotlib.pyplot as plt

D = 4.48e-11  # Diffusion coefficient
L = 50e-3  # Length of the sample 50 mm
Nx = 51
dx = L / (Nx - 1)
x = np.linspace(0, L, Nx)

T_total = 120 * 24 * 60 * 60  # Total simulation time in seconds
dt = 10 * 60  # Time step (10 minutes)
Nt = int(T_total / dt)  # Number of time steps

C = np.zeros(Nx)

# boundary condition
C_left_boundary_value = 0.165 # Surface concentration

for t in range(Nt):
    d2C_dx2 = np.gradient(np.gradient(C, dx), dx)

    C[0:-1] += dt * D * d2C_dx2[0:-1]

    C[0] = C_left_boundary_value

plt.plot(x, C)
plt.xlabel("x (m)")
plt.ylabel("C")
plt.title("Concentration Profile after 30 Days")
plt.show()
print(C)
```

8.3 Appendix 3

```
import numpy as np
import matplotlib.pyplot as plt

D = 1.53e-11  # diffusion coefficient in m^2/s
L = 0.05  # length of the sample in m
V = 20  # voltage in V
t_total = 24 * 60 * 60  # total time in s
z = -1  # ion valence for Cl-
F = 96485.33212  # Faraday's constant in C/mol
R = 8.314  # gas constant in J/(mol*K)
T = 298.15  # absolute temperature in K of room temperature
c_surface = 0.150  # surface concentration in mol/m^3
dx = 0.001  # spatial step in m
dt = 1  # time step in s
Nx = int(L/dx)  # number of spatial points
Nt = int(t_total/dt)  # number of time points
c = np.zeros((Nx, Nt))
c[0, :] = c_surface
phi = V * np.linspace(0, L, Nx) / L

for n in range(Nt-1):
    for i in range(1, Nx-1):
        d2c_dx2 = (c[i+1, n] - 2*c[i, n] + c[i-1, n]) / dx**2
        dc_dx = (c[i, n] - c[i-1, n]) / (dx)
        dphi_dx = (phi[i] - phi[i-1]) / (dx)
        dc_dt = D * (d2c_dx2 + (z * F / (R * T)) * dc_dx * dphi_dx)
        c[i, n+1] = c[i, n] + dt * dc_dt

plt.plot(np.linspace(0, L, Nx), c[:, -1])
plt.xlabel('Position (m)')
plt.ylabel('Concentration (mol/m^3)')
plt.title('Chloride concentration in the sample')
plt.show()
print(c[:, -1])
```